IEEE Open Journal of the
Industrial Electronics Society

Received 19 October 2022; accepted 14 November 2022. Date of publication 28 November 2022;
date of current version 19 December 2022. The review of this paper was arranged by Associate Editor Giovanni Spagnuolo.

Digital Object Identifier 10.1109/OJIES.2022.3225265

Survey of Topology Morphing Control Techniques for Performance Enhancement of Galvanically Isolated DC-DC Converters

VADIM SIDOROV[1] (Student Member, IEEE), ANDRII CHUB[1] (Senior Member, IEEE), DMITRI VINNIKOV[1] (Senior Member, IEEE), AND FANG Z. PENG[2] (Fellow, IEEE)

[1]Power Electronics Group, Department of Electrical Power Engineering and Mechatronics, Tallinn University of Technology, 12616 Tallinn, Estonia
[2]Department of Electrical and Computer Engineering, Florida State University, Tallahassee, FL 32306 USA

CORRESPONDING AUTHOR: DMITRI VINNIKOV (e-mail: dmitri.vinnikov@taltech.ee).

This work was supported in part by the Estonian Research Council under Grant PRG1086, and in part by the Estonian Centre of Excellence in Zero Energy and Resource Efficient Smart Buildings and Districts, ZEBE, under Grant 2014-2020.4.01.15-0016 funded by the European Regional Development Fund.

ABSTRACT This article provides a systematic survey on the topology morphing control techniques used in the galvanically isolated dc-dc converters. Existing techniques are broadly categorized based on the part where a converter changes its topology: at the input side, at the output side, and the advanced techniques that cannot be categorized in the first two groups. The techniques span from the simple reconfiguration between the full- and half-bridge switching cells similar to the conventional power supplies with universal ac input to the advanced multitrack topology and reconfigurable resonant tanks. In addition, the described variety of application examples proves the wide application range and versatility of the topology morphing control. These include fault tolerance, efficiency curve flattening, input voltage range extension, and other advantages. Hence, this article provides a single comprehensive source for researchers and engineers willing to enter the topic of topology morphing control.

INDEX TERMS Galvanically isolated dc-dc power converter, series resonant converters, topology morphing control.

I. INTRODUCTION

In recent years, widespread electrification has been considered the primary tool for more efficient energy generation and end-use due to the increase in renewable electric energy generation [1], [2]. DC distribution enables cost-efficient integration of renewable energy sources in comparison with the conventional ac systems [3], [4], [5], [6], [7]. The benefits of dc distribution are already justified in electric ships and vehicles, as well as electric aircrafts [6], [8], [9], [10]. The need for dc-dc converters combined with safety precautions led to intensive studies of galvanically isolated dc-dc topologies [11], [12].

The galvanically isolated dc-dc converters could be broadly categorized into three main classes: voltage–source, current–source, and impedance-source [12]. The voltage–source topologies are widely accepted by industry due to their simplicity, but they cannot withstand short-circuiting of the input capacitors and may require protection from misgatings. Contrary to that, the current–source topologies must avoid switching states that could interrupt the input inductor current. The impedance–source converters allow for any switching state, which increases their voltage regulation flexibility.

All these converters could be designed to be step-up when the output voltage is always higher than the input voltage, step-down when the output voltage is always lower than the input voltage, or step-up/down. From the voltage regulation point of view, the voltage–source topologies are essentially buck converters that have normalized dc voltage gain below one. The current–source topologies are boost converters that have normalized dc voltage gain above one. The impedance–source topologies could be either boost or buck-boost converters. Each converter type has performance limits, like limited input voltage regulation range, poor light load efficiency, power density, etc.

This work is licensed under a Creative Commons Attribution 4.0 License. For more information, see https://creativecommons.org/licenses/by/4.0/

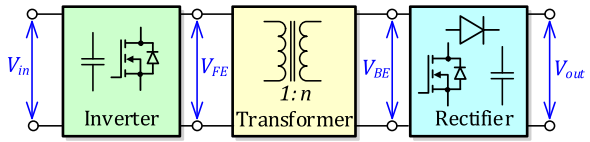

FIGURE 1. Generalized galvanically isolated dc-dc converter.

Optimization of converter hardware design is one possibility to improve converter performance by applying wide bandgap semiconductors or new magnetic materials [13], [14], [15]. Also, topologies could be hybridized to attain the benefits of several converter classes. For example, the buck-boost galvanically isolated dc-dc converter [16] is implemented by combining galvanically isolated boost impedance–source and buck series-resonant voltage–source dc-dc converter topologies.

Other possibilities of hardware design optimization include the following:

1) interleaved implementation of dc-dc converters, which allows for phase shedding at light loads for better efficiency;
2) integration of magnetic elements into a single planar component embedded in a PCB for higher power density;
3) switching frequency increased to MHz level along with soft-switching for high power density.

Converter performance optimization using advanced control is a new trend that provides cost-efficient results [17]. Typically, those are advanced nonlinear techniques, like model predictive control or sliding mode control. However, many converters can have several modes of operation. Therefore, control techniques that take advantage of the best characteristics of each mode are possible. Also, in conventional ac–dc power supplies, a full-bridge rectifier operating in 230 V ac grids can be reconfigured to a half-bridge (the voltage doubler) circuit that can operate in 120 V ac grids. This kind of control could be referred to as the topology morphing control (TMC).

The term "topology morphing control" first appeared in 2015 [18], while some of the concepts covered in this review date back to 2005. The topology morphing control is realized by the online reconfiguration of a converter topology to extend voltage or power ranges or to provide fault tolerance without changing the hardware. The switching between discontinuous and continuous conduction modes is not TMC. Hence, it is essential to provide a systematic survey on this topic to cover different existing converters that can be categorized as those employing the TMC. This survey systematizes and organizes this topic for the first time to provide a single point of reference for engineers and researchers.

Furthermore, the article compares all existing TMC techniques and provides recommendations for applying TMC in different application cases. The article is organized as follows. Section II explains the essence of the TMC. Section III covers the known TMC applications at the input side of galvanically isolated dc-dc converters. Section IV describes different reconfigurable rectifiers that could be utilized on the output side. Other advanced techniques that cannot be categorized in the first two groups are covered in Section V. Section VI illustrates how TMC can be used in the galvanically isolated dc-dc converters and which performance indicators could be improved. Finally, Section VIII concludes this article.

II. MAIN PRINCIPLE OF TMC

Typically, galvanically isolated dc-dc converters consist of a high-frequency front-end inverter, an isolation transformer, and a back-end rectifier (see Fig. 1). Hence, the converter dc voltage gain could be defined as follows:

$$G = \frac{V_{\text{out}}}{V_{\text{in}}} = G_{FE} \cdot G_{TX} \cdot G_{BE} \tag{1}$$

where G_{FE} is the voltage gain of the front-end inverter defined as the ratio between the peak-to-peak voltage applied to the transformer and the double of the input voltage

$$G_{FE} = \frac{V_{FE(pk-pk)}}{2V_{\text{in}}} \tag{2}$$

$G_{TX} = n$ is the turns ratio of the isolating transformer; G_{BE} is the voltage gain of the back-end rectifier defined as the ratio between the double of the output voltage and the peak-to-peak voltage fed by the isolation transformer

$$G_{BE} = \frac{2V_{\text{out}}}{V_{BE(pk-pk)}}. \tag{3}$$

Typically, these gain values are constant. However, applying TMC in any stage allows for regulating these values, typically in integer steps. This article outlines reconfiguration in different stages that can bring different benefits.

Based on these definitions, a classification of TMC techniques could be derived, as shown in Fig. 2. Among the known techniques, the application of two- and three-level full-bridge inverters (FBIs) was found in the literature. The two-level FBIs typically employ reconfiguration from the full-bridge to another mode with less active switches, like half-bridge, flyback, or forward. On the other hand, the three-level FBIs could feature at least three different operation modes. Similarly, multimode rectifiers could be active two- and three-level circuits or passive voltage multipliers with static switches reconfiguring their gain/mode. Some of them can reach up to sixfold gain, but only up to four different modes were observed for some of them in the literature.

Static reconfiguration of the input or output stages is a typical TMC approach. However, more advanced techniques are available too. First, some rectifiers could contain switches controlled at the switching frequency while still providing static dc gain control by changing switching patterns, achieving up to two TMC modes. A wide range of techniques also manipulate the transformer turns ratio G_{TX}. These techniques are referred to as advanced TMC techniques as they typically involve two transformation stages and changing front-end

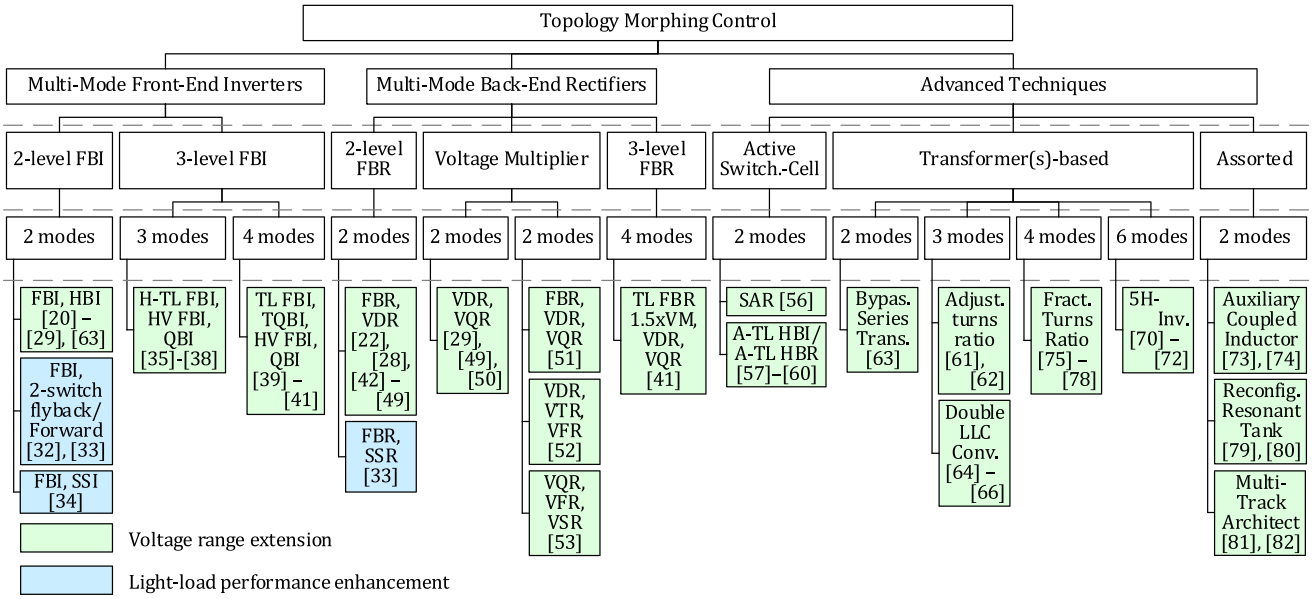

FIGURE 2. Classification of the TMC techniques.

inverter stage switching patterns. Some of them could be complicated due to the implementation of six possible operating modes.

The last group of the assorted advanced TMC techniques is not categorized based on their unique implementation. They include the reconfiguration of the resonant tank using a bidirectional switch, the use of auxiliary inductor winding to establish an additional power transfer link between the input and output sides, and cascaded integration of several typical switching cells to create a versatile multitrack dc-dc architecture.

As shown in Fig. 2, all the techniques included in this survey can be broadly categorized into two main groups. First, most TMC techniques target the dc voltage regulation range extension. However, they could also be used for achieving fault-tolerance when a converter needs to recover its operation by modifying gains of the dc-dc converter parts to compensate for damaged components. On the other hand, some TMC techniques target switching power loss reduction at light load to flatten the converter efficiency curve across its input power range.

The following sections follow the generalized classification of the TMC techniques. Therefore, the next section covers different reconfiguration types of the high-frequency front-end inverter.

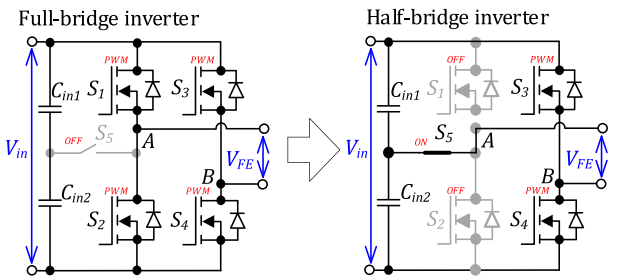

FIGURE 3. Reconfiguration of the front-end inverter with an additional switch from the full-bridge to the symmetrical half-bridge.

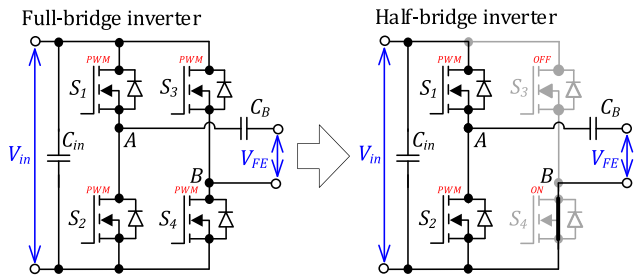

FIGURE 4. Reconfiguration of the front-end inverter with the blocking capacitor from the full-bridge to the asymmetrical half-bridge.

III. INPUT SIDE TMC TECHNIQUES

A. FULL-BRIDGE INVERTER TO HALF-BRIDGE INVERTER

The most widespread example of the TMC at the input side of galvanically isolated dc-dc converters is the reconfiguration from a FBI to a half-bridge inverter (HBI). It can be realized using a capacitor leg (C_{in1} and C_{in2}) and an additional switch S_5 (see Fig. 3), or by a blocking capacitor C_B (see Fig. 4). In the first case, the additional switch S_5 is bidirectional and can be an electromechanical relay or two series MOSFETS [19], [20], [21], [22]. In the FBI mode, the switch S_5 is turned OFF; in the HBI mode, the switch S_5 is turned ON, and one transistor leg (S_1 and S_2) is turned OFF (see Fig. 5).

Usually, the series blocking capacitor is utilized in resonant topologies, such as the LLC, the CLLC, or the series resonant converters (SRC) [19], [23], [24], [25], [26], [27], [28], [62]. In the HBI, one switch in one leg could be turned ON

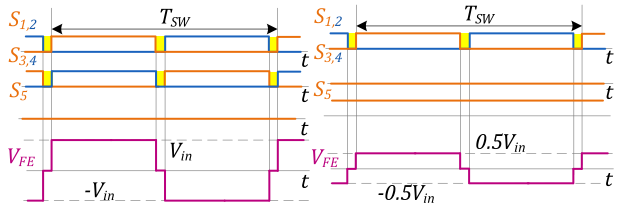

FIGURE 5. Operation of the front-end inverter with an additional switch as (a) FBI and (b) HBI.

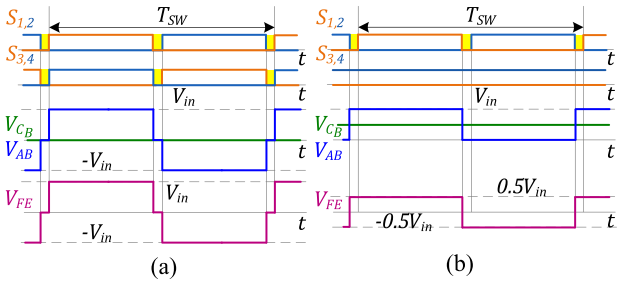

FIGURE 6. Operation of the front-end inverter with the blocking capacitor as (a) FBI and (b) HBI.

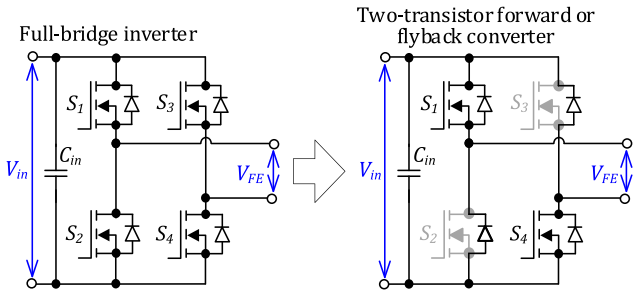

FIGURE 7. Reconfiguration of the front-end inverter from the full-bridge to the two-transistor forward or flyback inverter.

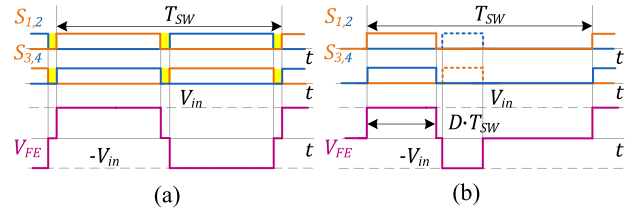

FIGURE 8. Operation of the (a) FBI and (b) two-transistor forward or flyback inverter.

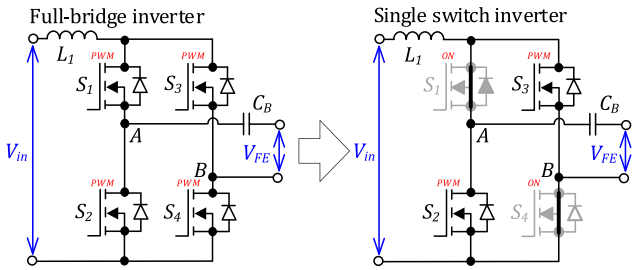

FIGURE 9. Reconfiguration of the front-end inverter from the full-bridge to the single-switch inverter.

continuously, while the other one is turned OFF. As a result, the average voltage of the blocking capacitor C_B equals half the input voltage. The amplitude of the inverter output voltage equals $V_{FE} = \pm 0.5V_{\text{in}}$ (see Fig. 6). In both cases, the reconfiguration of the inverter from the FBI to the HBI changes the voltage gain G_{FE} from 1 to 0.5. Therefore, the HBI mode can double the input or output voltage range. However, RMS currents in the blocking capacitor, the primary winding of a transformer, and the switch S_4 are increased $\sqrt{2}$ times at the same operating point. It should be considered in the thermal design of the converter.

Frequency modulation (FM) or symmetrical or asymmetrical pulse-width modulations (PWM or APWM) with fixed switching frequency could be applied to regulate the voltage gain in the HBI mode, depending on the converter topology. At the same time, FM and different types of PWM or phase-shift modulations can be applied in the FBI mode [30].

B. FULL-BRIDGE INVERTER TO THE FLYBACK OR FORWARD MODE

In the next example, the TMC is reconfigured from the FBI into the two-transistor forward or the two-transistor flyback converter (see Fig. 7). The type of a reconfigurable converter depends on the type of an isolation transformer. The reconfiguration into the two-transistor forward and flyback converters is exemplified in [31] and [32], respectively. Reconfiguration to the forward or the flyback mode in the light load conditions provides lower switching and gate-driver losses (two switching devices versus four devices). According to the study, these reconfigurations improve the light-load efficiency of a converter by up to 40%. Fig. 8 shows control signals of switches in the FBI mode and the two-transistor forward or flyback mode. In the two-transistor forward and flyback modes, body diodes of switches S_3 and S_2 conduct the transformer current when the active switches S_1 and S_4 have been turned OFF and the magnetizing current decreases to zero. It is the main drawback of the two-transistor forward and flyback modes because the forward voltage and reverse recovery losses could be relatively high in the body diodes.

C. FULL-BRIDGE INVERTER TO SINGLE-SWITCH INVERTER

The following example of the TMC is the reconfiguration of the FBI to the single-switch inverter (SSI), as shown in Fig. 9. This TMC is possible only in the current- and impedance-source topologies with an inductor or an impedance-source network at the input, such as quasi-Z-source networks described in [33]. In the SSI mode, diagonal switches (for

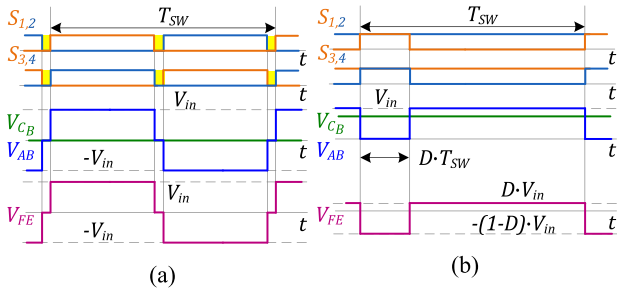

FIGURE 10. Operation of the FBI (a) before and (b) after its reconfiguration into SSI.

example, S_1 and S_4) are turned ON continuously, and the inverter operates as the buck-boost converter with the nominal gain that equals $G_{FE} = 1$ at the duty cycle $D = 0.25$.

The other diagonal switches (S_2 and S_3) are operating during the duty cycle, thus shorting the inverter (see Fig. 10). The blocking capacitor C_B balances the voltage applied to a transformer as in the HBI mode. According to the study [33], the SSI has higher performance at a light load and higher input voltage than the FBI. The main disadvantage of this TMC is high current stress in the diagonal switches S_1 and S_4.

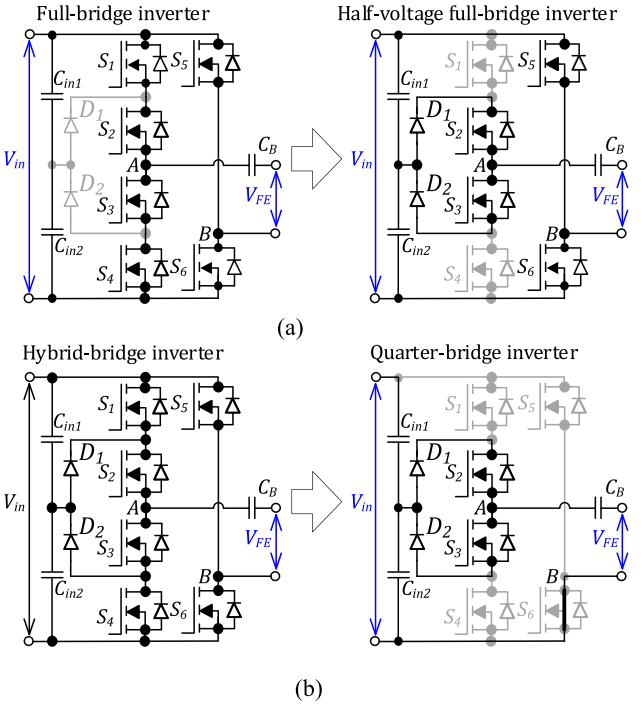

FIGURE 11. Reconfiguration of the hybrid three-level inverter from (a) FBI to HV FBI mode and (b) QBI mode.

D. HYBRID THREE-LEVEL FULL-BRIDGE INVERTER TO HALF-VOLTAGE FULL-BRIDGE INVERTER AND QUARTER-BRIDGE INVERTER

In high-voltage applications, three-level inverters (TLIs) are a solution to the voltage stress reduction of the switching devices. Though the three-level inverters are complex, low voltage rating power MOSFETS feature low cost, low drain–source ON-state resistance, and low output capacitance. As a result, conduction and switching losses can be reduced compared to a full-bridge converter with high voltage rating power switches. In addition, a complex circuit of the TLI facilitates flexible control and the TMC. The first example of the TMC in three-level inverters is the reconfiguration of a hybrid three-level inverter (H-TLI) from the FBI mode to the half-voltage FBI (HV FBI) mode [34], [35], [36], [37]. Besides, the blocking capacitor C_b allows for operating in the quarter bridge inverter (QBI) mode.

One leg of the H-TLI consists of two transistors like the conventional FBI, and the other leg consists of four switches, two diodes, and two capacitors, as shown in Fig. 11. The operation principle of the H-TLI in four modes is shown in Fig. 12. In the HV FBI mode, half of the input voltage on capacitors $C_{\text{in}1}$ and $C_{\text{in}2}$ is applied between points A and B through a diode D_1 or D_2. In the HV FBI mode, the nominal voltage gain equals $G_{FE} = 0.5$. Also, the H-TLI can operate in the hybrid three-level mode, where the gain is regulated in the range $G_{FE} = 0.5 \ldots 1$ by the variation of a duty cycle D [see Fig. 12(c)]. In the QBI mode, the gain equals $G_{FE} = 0.25$. The H-TLI can operate in three nominal points: $G_{FE} = 1$, 0.5, and 0.25. The main disadvantages of TLIs are challenging converter optimization and the high complexity of the circuits related to the control and driving of switches.

TLIs require many isolated auxiliary supplies for each transistor. Another disadvantage of the H-TLI is that it has two different types of transistors because the voltage stress equals half the input voltage in the first leg and the full input voltage in the other leg.

E. THREE-LEVEL FULL-BRIDGE INVERTER TO THREE-QUARTERS BRIDGE INVERTER, TO HALF-VOLTAGE FULL-BRIDGE INVERTER, AND QUARTER-BRIDGE INVERTER

The latest example of the TMC in three-level inverters is the reconfiguration of the three-level full-bridge inverter (TL FBI), which can operate in four modes: the FBI, the three-quarter bridge inverter (TQBI), the HV FBI, and the QBI mode, as described in [38], [39], [40]. Terms like TQBI reflect the main characteristic of the front-end inverter—its dc-ac voltage gain. TL FBI consists of two four-transistor legs ($S_1 \ldots S_8$), flying capacitors (C_{f1} and C_{f2}), two input capacitors ($C_{\text{in}1}$ and $C_{\text{in}2}$), and four diodes ($D_1 \ldots D_4$).

This example is suitable for high voltage applications with a wide voltage gain range. Flying capacitors help with the voltage balancing across the switches. The voltage of the flying capacitors equals $0.5V_{\text{in}}$. Flying capacitors do not conduct current only in the FBI mode. In the other modes, it is necessary to control the voltage of the flying capacitors by alternating the active transistors. An implementation example of this TMC technique is shown in Fig. 13. The dc-ac voltage gains in the FBI, the TQBI, the HV FBI, and the QBI mode

TABLE 1 Comparison of TMC at the Input Side

TMC	Nominal voltage gain G_{FE}	Number of components[1]			Cost[2]	Advantage	Disadvantage	Application examples		
		S	D	C				Input dc voltage, V	Output dc voltage, V	Power, W
FBI to HBI (Fig. 5)	1; 0.5	4	0	2	$	Voltage gain range extension up to two times	High current stress in one switch	100–400	48	800 [19]
								120–240	24	480 [20]
								30–60	200/400 V	500 [21]
								120–240	96	1000 [22]
								600	180–540	1400 [26]
								150–400	1650	2500 [28]
FBI to 2T-flyback or 2T-forward (Fig. 7)	1	4	0	1	$	Light-load efficiency enhancement (+5 %)	High conduction and reverse recovery losses in body diodes	36	200	20–300 [31]
								20–30	170/ 200–270	10–100 [32]
FBI to SSI (Fig. 9)	1	4	0	L=1	$	Light-load efficiency enhancement (+3 %)	High current stress in the diagonal switches	10–60	400	25–250 [33]
H-TL FBI to HV FBI, to QBI (Fig. 11)	1; 0.5; 0.25	6	2	2	$$	Voltage gain range extension up to four times	Unequal voltage and current stress in switches	200–400	360	1500 [34]
								240–480	30–60	1200 [35]
								385	225–378	6600 [36]
								200–400	60	1200 [37]
TL FBI to TQBI, to HV FBI, to QBI (Fig. 13)	1; 0.75; 0.5; 0.25	8	4	4	$$$	Voltage gain range extension up to six times	High number of switches, unequal current stress in switches	750	50–600	20 000 [38]
								100	20–100	500 [39]
								200	200–700	3500 [40]

Note: [1]S=switch; D=diode; C=capacitor; L=inductor.
[2]Estimated cost: $ is a low cost; $$ is a medium cost; $$$ is a high cost.

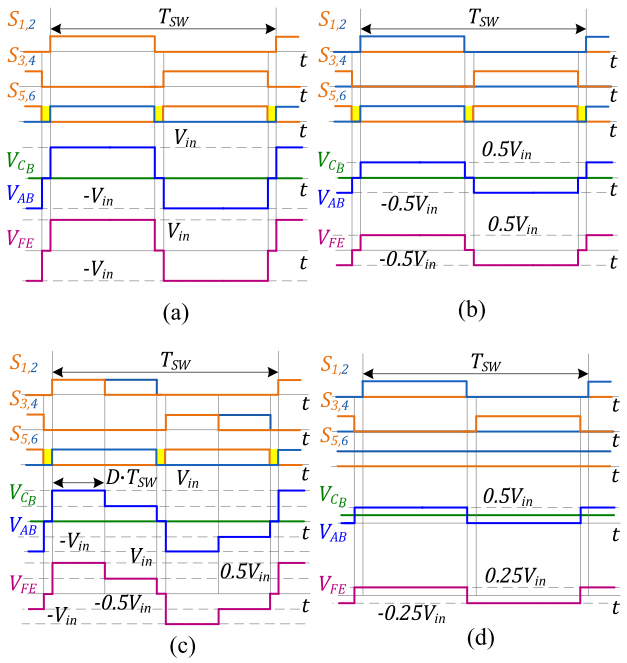

FIGURE 12. Operation of the hybrid three-level inverter as (a) FBI, (b) HV FBI, (c) hybrid three-level inverter, and (d) QBI.

equal 1, 0.75, 0.5, and 0.25 (see Fig. 14), respectively. This TL inverter type features the largest number of nominal voltage gains. However, three-level resonant converters working with a wide input/output voltage range still encounter many difficulties, including high conducting losses, challenging converter optimization, and high circuit complexity related to the control and power stage.

F. SUMMARY

The TMC techniques in the front-end inverters are compared in Table 1. Nominal voltage gain values are reference values that do not consider modulation necessary to achieve gain values between them. The input-side TMC techniques, such as reconfigurations of the FBI to the two-switch flyback or forward mode or the SSI, enhance efficiency at a light load. Other examples extend the voltage gain range and improve performance in a wide range of voltage gain.

The voltage gain extension could be easily achieved in the given techniques as the front-end inverter defines the voltage swing applied to the isolation transformer. However, in some cases, reducing the number of active switches could reduce switching losses at a light load, resulting in efficiency enhancement. The literature shows that two-mode techniques, like reconfiguring the FBI into HBI, could yield sufficient performance for most applications. Multimode topologies derived from TL FBI could be used in niche applications where the dc voltage gain is wide and the maximum operating voltage is high. Considering asymmetrical maximum voltage and current stress of semiconductor devices, future research should target new design approaches tailored to applications by proper dimensioning of the semiconductors and corresponding cooling system.

IV. OUTPUT SIDE TMC TECHNIQUES

TMC can also be applied at the output of galvanically isolated dc-dc converters. Besides, inverters with TMC can operate

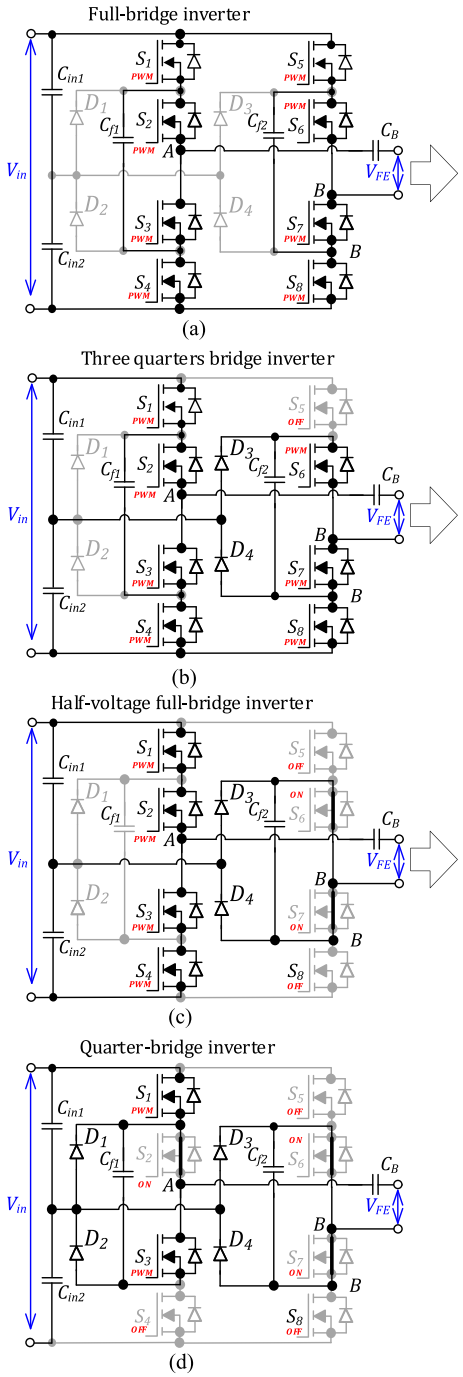

FIGURE 13. Reconfiguration of the three-level full-bridge inverter from (a) FBI to (b) TQBI, to (c) HV FBI, and to (d) QBI mode.

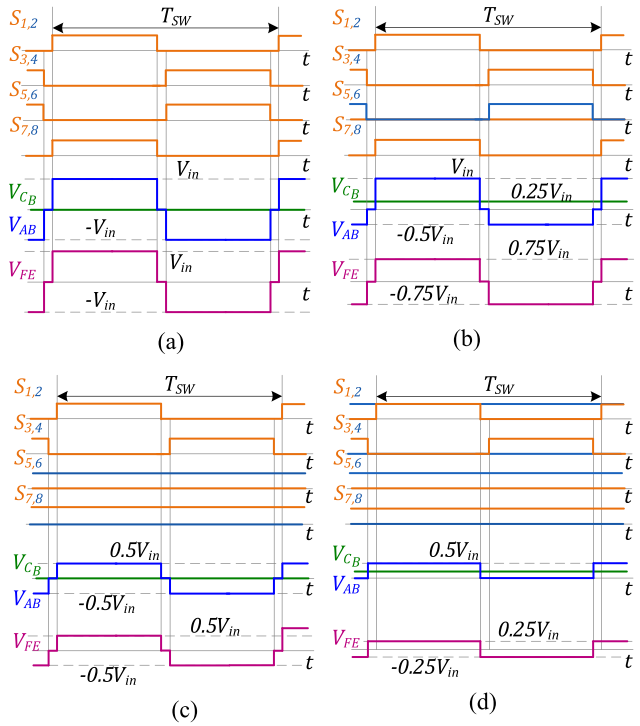

FIGURE 14. Operation of the three-level full-bridge inverter as FBI (a), half-voltage FBI (b), hybrid three-level inverter (c), and QBI (d).

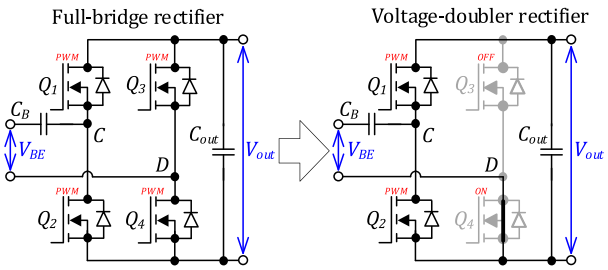

FIGURE 15. Reconfiguration of the back-end rectifier with the blocking capacitor from the full-bridge to the half-bridge.

as a rectifier in the backward power flow direction. In this case, presumably, all examples of the TMC in inverters can be considered for rectifiers.

A. FULL-BRIDGE RECTIFIER TO VOLTAGE-DOUBLER RECTIFIER

The first example of TMC at the output side is a transition from the full-bridge rectifier (FBR) to the half-bridge rectifier (HBR), also known as the voltage-doubler rectifier (VDR). This TMC can be realized by the capacitor leg and an additional switch [41], [42], [43], [44] or the blocking capacitor [21], [27], [45], [46], [48], similar to the FBI–HBI reconfiguration described in the previous section. Fig. 15 shows the reconfiguration from the FBR to the VDR with the blocking capacitor. The rectifier operation after the reconfiguration is the same as the operation of the half-bridge inverter (see Fig. 16). In the FBR mode, all transistors operate as a synchronous rectifier; in the VDR mode, two switches, Q_1 and Q_2, operate as a rectifier. The voltage gain of the rectifier in the FBR mode equals $G_{BE} = 1$, and the gain in the VDR mode equals $G_{BE} = 2$. In the VDR mode, the current stress of the blocking capacitor and the switch Q_4 are two times higher than that in the FBR mode.

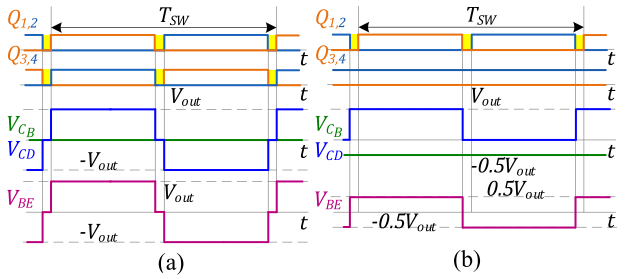

FIGURE 16. Operation of the back-end rectifier with the blocking capacitor as (a) FBR and (b) VDR.

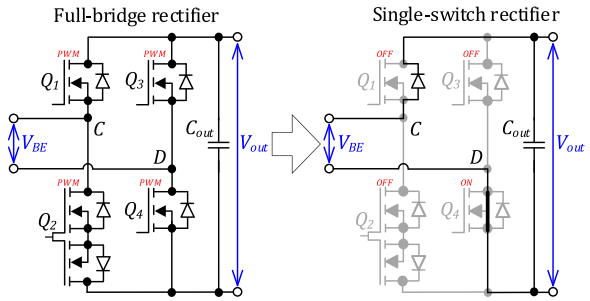

FIGURE 17. Reconfiguration of the back-end rectifier with a bidirectional switch from the full-bridge to the single-switch rectifier.

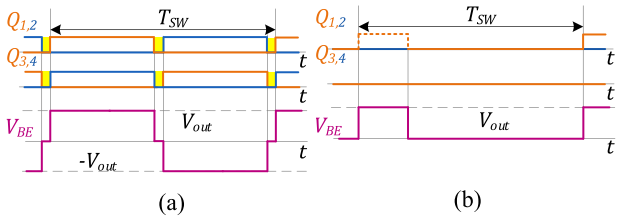

FIGURE 18. Operation of the back-end rectifier with a bidirectional switch as (a) FBR and (b) SSR.

B. FULL-BRIDGE RECTIFIER TO SINGLE-SWITCH RECTIFIER

This TMC technique is based on the rectifier reconfiguration from the FBR to a single-switch rectifier (SSR), also called a half-wave rectifier. Terminology-wise, the SSR shows the duality between TMC application at the input and output sides. This type of TMC requires a bidirectional switch Q_2 in one rectifier leg for blocking this conduction path (see Fig. 17). A switch Q_4 in another leg is turned ON continuously, and the switches Q_1 and Q_3 are turned OFF. Thus, only the body diode of switch Q_1 operates in the SSR mode, or switch Q_1 operates as a synchronous rectifier (see Fig. 18). SSR is suitable for operation as a rectifier of the flyback converter. For example, in [32], the inverter is reconfigured from the FBI to the two-switch flyback converter. At the same time, the rectifier is reconfigured from the FBR to the SSR. This TMC allows for improving performance at a light load. The voltage gain in both modes is the same. However, using the bidirectional switch is a drawback of this TMC technique.

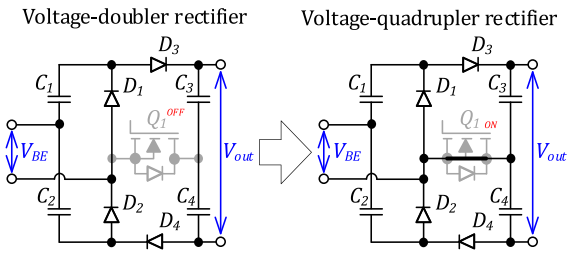

FIGURE 19. Reconfiguration of the back-end rectifier with an NPC switch from VDR to VQR.

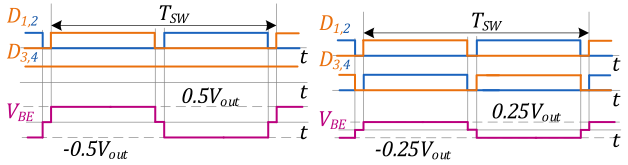

FIGURE 20. Operation of the back-end rectifier with an NPC switch as (a) VDR and (b) VQR.

C. VOLTAGE-DOUBLER RECTIFIER TO VOLTAGE-QUADRUPLER RECTIFIER

The third example of TMC at the output side is the VDR reconfiguration into the voltage-quadrupler rectifier (VQR) [28], [48], [49], as shown in Fig. 19. In this circuit, the NPC switch Q_1 operates in ON/OFF mode and selects the mode of the rectifier. The diodes D_3 and D_4 are required in the VQR mode for blocking the reverse current. The capacitors C_3 and C_4 perform second voltage doubling in the VQR mode and operate as the output filter in the VDR mode. The operation principle of the diodes and the switch under both modes is shown in Fig. 20. In this figure and further in the article, active levels for diodes show when they are expected to conduct current under ideal conditions.

The voltage gain of the rectifier equals $G_{BE} = 4$ in the VQR mode. In the VQR mode, the current stress of the blocking capacitor and the switch Q_4 is two times higher than that in the VDR mode, which is the drawback of this TMC.

D. FULL-BRIDGE RECTIFIER TO VOLTAGE-DOUBLER RECTIFIER AND VOLTAGE-QUADRUPLER RECTIFIER

The combination of the first and the third case of the TMC at the output side is described in [50]. This example shows reconfiguration between the FBR, the VDR, and the VQR (see Fig. 21). The circuit of the rectifier consists of six diodes, four capacitors, two of which are blocking, and two transistors operate in the ON/OFF mode. TMC is implemented by switching the transistors: both transistors are turned off in the FBR mode (but the body diode of the Q_2 conducts current), the transistor Q_1 is turned ON in the VDR mode, and both transistors are turned ON in the VQR mode, as shown in Fig. 22. In some modes, only part of the circuit is operational. For example, diodes D_3 and D_4, the blocking capacitor C_{B2}, and the capacitor C_2 operate only in the VQR mode. At the same

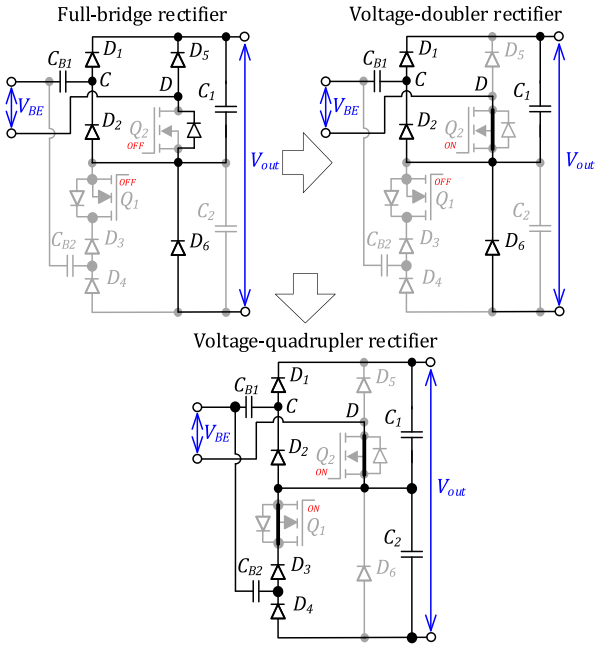

FIGURE 21. Reconfiguration of the three-mode back-end rectifier from the FBR to the VDR and the VQR.

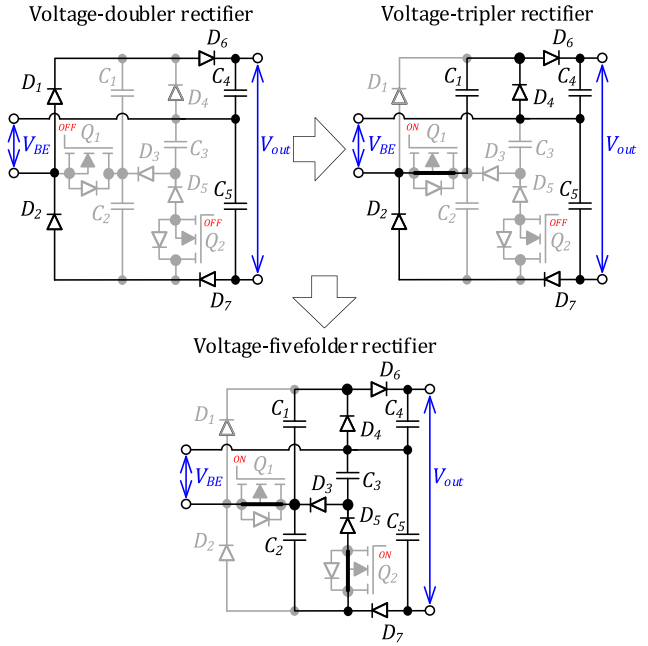

FIGURE 23. Reconfiguration of the three-mode back-end rectifier from VDR to VTR and VFR.

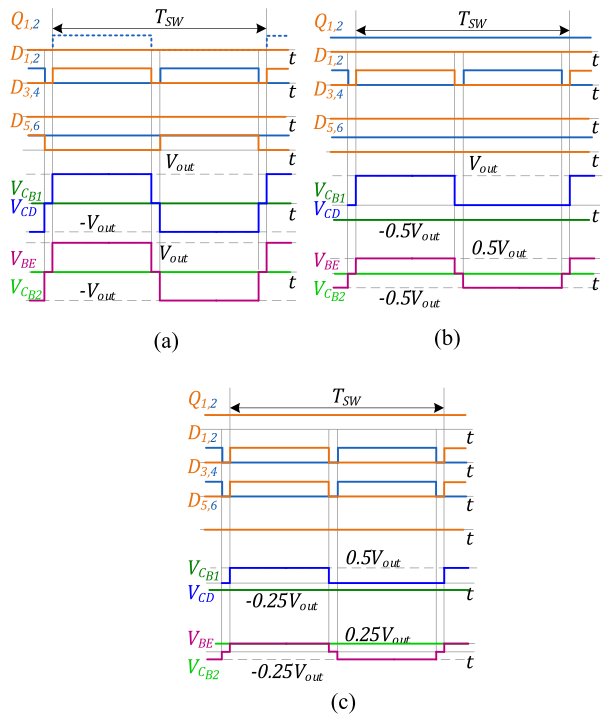

FIGURE 22. Operation of the three-mode back-end rectifier as (a) FBR, (b) VDR, and (c) VQR.

time, the diode D_5 operates only in the FBR mode. The main advantage of this example is the wide voltage gain range of the rectifier, considering that the voltage gain equals G_{BE}=1, 2, and 4. Drawbacks of this approach are a large number of semiconductor devices, unequal current stress of diodes, and high current stress of components in the VQR mode. In each mode, two diodes and one transistor conduct the current, increasing the parasitic series equivalent resistance of the rectifier. These drawbacks can be neutralized by selecting suitable semiconductor devices and the thermal design of the rectifier.

E. VOLTAGE-DOUBLER RECTIFIER TO VOLTAGE-TRIPLER RECTIFIER AND TO VOLTAGE-FIVEFOLDER RECTIFIER

An alternative implementation of a three-mode rectifier was proposed in [51]. It can operate in the VDR, the voltage-tripler rectifier (VTR), and the voltage-fivefolder rectifier (VFR) modes (see Fig. 23). The proposed rectifier consists of seven diodes, five capacitors, and two transistors. As in previous examples, the transistors operate in the ON/OFF mode and control the rectifier mode. In the VDR mode, both transistors are turned OFF; in the VTR mode, the Q_1 is turned ON; in the VFR mode, both transistors are turned on. Depending on the operation mode, the voltage gain of the rectifier can equal G_{BE} = 2, 3, and 5. Though the voltage gain in the VFR mode is high, the voltage gain range of this reconfigurable rectifier is not as wide as in the previous example. The high number of utilized components is the main drawback of this reconfigurable rectifier. Also, three diodes simultaneously conduct current in the VTR and VFR modes (see Fig. 24). This feature increases conduction losses and requires using Schottky diodes with low forward voltage.

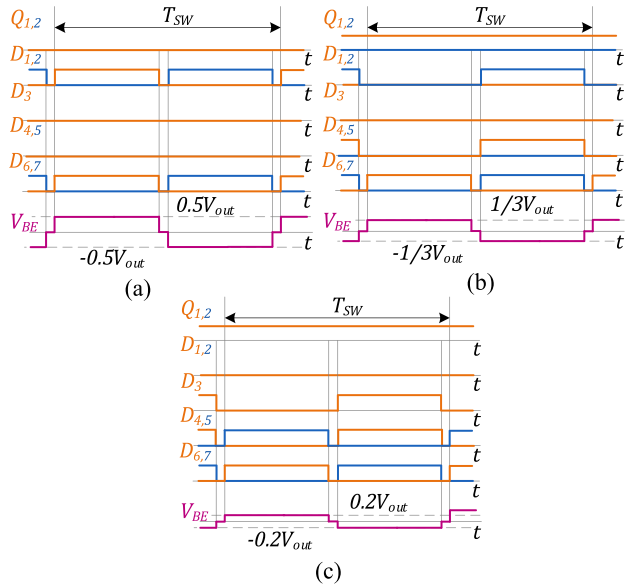

FIGURE. 24. Operation of the three-mode back-end rectifier as (a) VDR, (b) VTR, and (c) VFR.

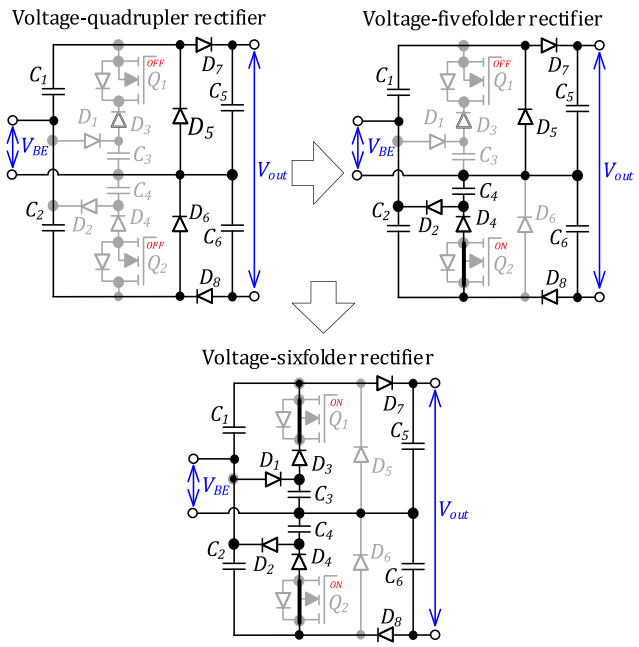

FIGURE 25. Reconfiguration of the three-mode back-end rectifier from VQR to VFR and VSR.

F. VOLTAGE-QUADRUPLER RECTIFIER TO VOLTAGE-FIVEFOLDER RECTIFIER AND VOLTAGE-SIXFOLDER RECTIFIER

The study in [52] presents a rectifier operating in the VQR, the VFR, and the voltage-sixfolder rectifier (VSR) modes (see Fig. 25). Mode is selected by turning ON/OFF the static transistors like in the previous case. Fig. 26 explains the operation of switches and diodes in different modes. In the listed

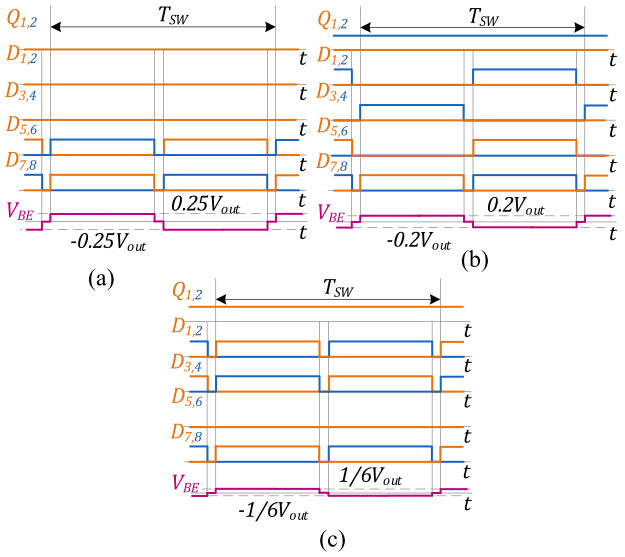

FIGURE 26. Operation of the three-mode back-end rectifier as (a) VQR, (b) VFR, and (c) VSR.

modes, the voltage gain of the rectifier G_{BE} equals 4, 5, and 6. Although the voltage gain has high values, the voltage gain range is not as wide as in the previous three-mode rectifiers. At the same time, compared with the previous examples, component count is the largest: eight diodes, six capacitors, and two transistors, which is a serious drawback of this approach.

G. THREE-LEVEL FULL-BRIDGE RECTIFIER TO 1.5-TIMES VOLTAGE MULTIPLIER, TO VOLTAGE-DOUBLER RECTIFIER, AND VOLTAGE-QUADRUPLER RECTIFIER

In high-voltage applications, three-level rectifiers can be applied to decrease the voltage stress of the components and, as a result, reduce component costs. The three-level inverters, such as the TL HBI and the TL FBI, can be used as rectifiers. An example of using the three-level full-bridge rectifier (TL FBR) is described in [40]. The operation principle is similar to that of the TL FBI. Depending on the modulation, the rectifier can operate as the FBR, the 1.5-times voltage multiplier (1.5xVM), the VDR, or the VQR, as shown in Fig. 27. The voltage gain G_{BE} equals 1, 1.5, 2, and 4 in the mentioned modes. At the same time, the average voltage of the blocking capacitor V_{Cb} equals zero in the FBR and the VDR modes and $0.25V_{\text{out}}$ in the $1.5\times$VM and the VQR modes, respectively (see Fig. 28). The voltage stress of the components is equal to half the output voltage. The drawback of this approach is the highest component count and the most complex circuit of the rectifiers described above.

H. SUMMARY

The topology morphing control in the back-end rectifiers is compared in Table 2. The nominal voltage gain values are defined by the converter operating points when no boost or buck voltage regulation is performed, which is similar to the converter operation as a dc transformer. The dc gain values

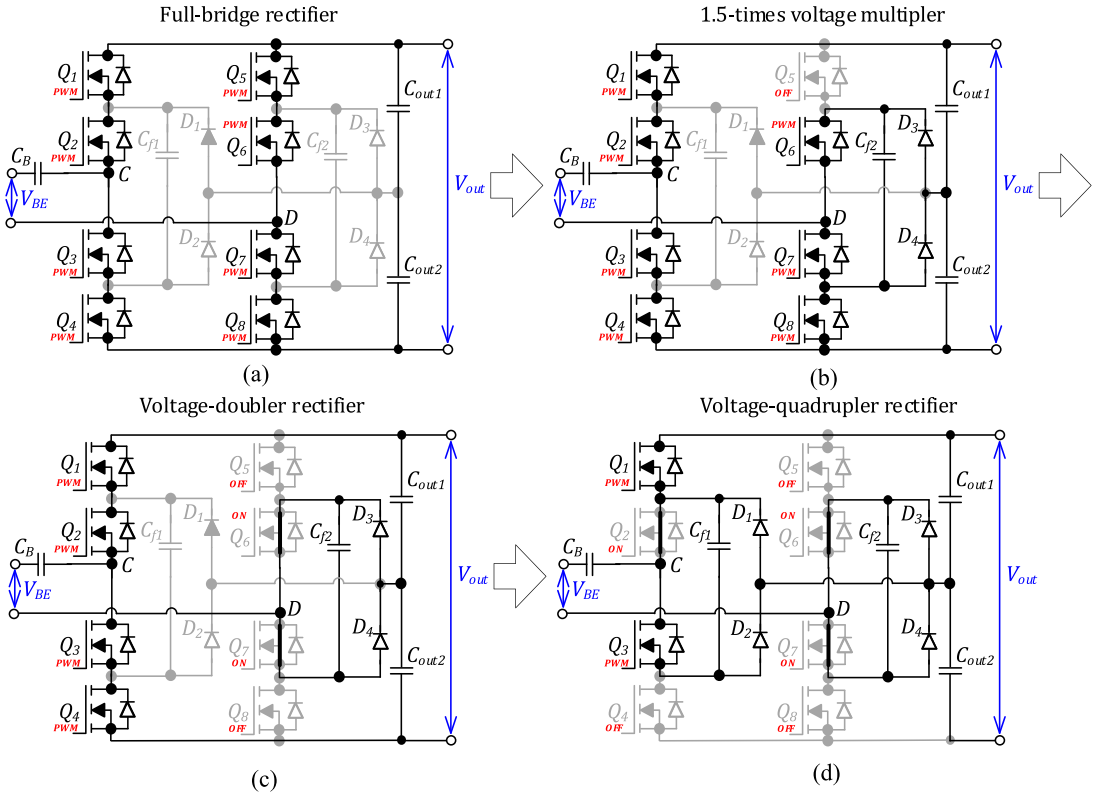

FIGURE 27. Reconfiguration of the three-level half-bridge rectifier from (a) the FBR to (b) the 1.5xVM, (c) the VDR, and (d) the VQR.

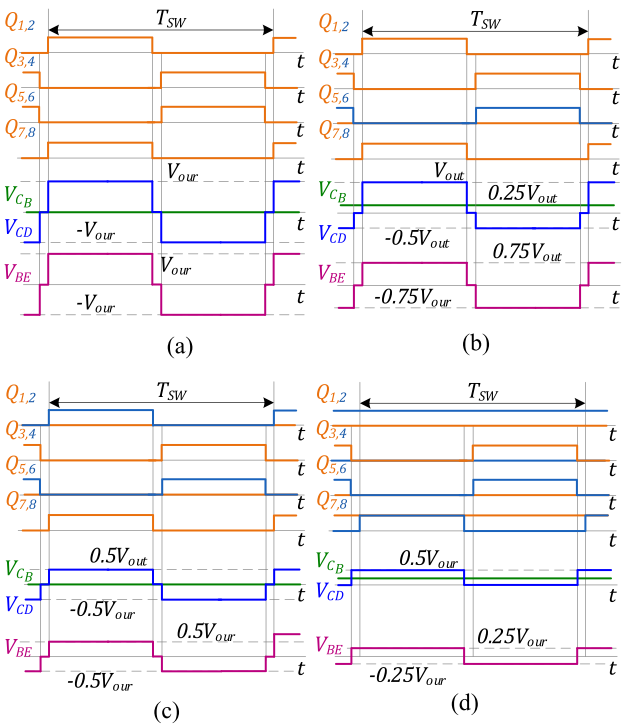

FIGURE 28. Operation of the three-level half-bridge rectifier as the (a) FBI, (b) the VDR, (c) the 1.5xVM, and (d) the VQR.

between them could be achieved only by implementing boost or buck voltage regulation using a pulsewidth or frequency modulation.

Most of the case studies in the techniques surveyed were dedicated to extending the converter gain range, with the fourfold extension being the best-reported result. Only one technique that applies SSR as one of the modes was used to enhance the efficiency, but it was combined with the corresponding input-side reconfiguration. Hence, the resulting efficiency improvement cannot be associated with the rectifier reconfiguration alone. Most of the techniques implement integer steps in the rectifier ac–dc gain G_{BE}, which makes them useful for the extension of the regulation range. The gain steps allow for keeping the control variable of the front-end inverter in the range of favorable efficiency, as it does not need to regulate the input voltage more than twofold before the rectifier changes its mode again. However, the mode changes could result from the considerable input and output voltage or current transients.

These techniques typically yield no significant efficiency improvement. Instead, they allow keeping its values in a wider input voltage range where a converter would not be able to operate due to limits of its input voltage regulation and power loss dissipation. In particular, full-bridge step-up dc-dc converters typically feature efficiency rising with the input

TABLE 2 Comparison of TMC at the Output Side

TMC	Nominal voltage gain G_{BE}	Number of components[1]			Cost[2]	Advantage	Disadvantage	Application examples		
		S	D	C				Input dc voltage, V	Output dc voltage, V	Power, W
FBR to VDR (Fig. 15)	1; 2	4	0	2	$	Voltage gain range extension up to two times	High current stress in one switch and blocking capacitor	30–60	200/400 V	500 [21]
								390	250–450	900
								17–43	340–430	250
								400	100–420	1500
								36–60	340–380	800
								18–36	12	120
								800	200–950	3300 [46]
FBR to SSR (Fig. 17)	1	4	0	1	$	Light-load efficiency enhancement (+8%)	High conduction and reverse recovery losses in body diodes	20–30	170/ 200–270	10–100 [32]
VDR to VQR (Fig. 19)	2;4	1	3	4	$	Voltage gain range extension up to two times	High current stress in one switch and blocking capacitor	150–400	1650	2500 [28]
								300–700	6600	2500 [49]
FBR to VDR, to VQR (Fig. 21)	1;2;4	2	6	4	$$	Voltage gain range extension by 4 times, reduced voltage stress by two times	High number of semiconductors, unequal current stress of diodes, and high current stress of components	5–110	400	360 [50]
VDR to VTR, to VFR (Fig. 23)	2; 3; 5	2	7	5	$$	Voltage gain range extension by 2.5 times, voltage stress by 2 times	High number of utilized components, high current stress in diodes.	25–100	500	250 [51]
VQR to VFR, to VSR (Fig. 25)	4; 5; 6	2	8	6	$$	Voltage gain range extension by 1.5 times	High number of switches, unequal current stress in switches	25–50	760	300 [52]
TL FBR to 1.5xVM, to VDR, to VQR (Fig. 27)	1; 1.5; 2; 4;	8	4	4	$$$	Voltage gain range extension up to four times, reduced voltage stress by 2 times		200	200–700	3500 [40]

Note: [1]S=switch; D=diode; C=capacitor; L=inductor.
[2]Estimated cost: $ is a low cost; $$ is a medium cost; $$$ is a high cost.

voltage, which could result in significant efficiency ripple at the rectifier mode transitions [53]. Such a step in the converter losses at the mode change could compromise the converter reliability due to the thermal cycling of components. Therefore, the reconfigurable rectifiers are much more suitable for application with front-end inverters featuring a reduced number of components, like HBI or SSI, as those feature symmetrical efficiency curves regarding the middle of their duty cycle regulation range. Contrary to this, the resonant converters with dc voltage gain close to one show much lower efficiency variation in their typical regulation range. The application of reconfigurable rectifiers could extend their voltage gain range while keeping a relatively flat efficiency curve.

More complicated circuits based on the three-level FBR could be useful in applications where the output voltage must vary in a wide range, reaching values above the blocking capacity of a single device. An example of such an application could be the electric vehicle charging standard CHAdeMO, which requires the charging voltage range from 50 to 1000 V [54].

The most critical points to be addressed are achieving a smooth transition between the modes and assessment of the associated damage accumulation in the converter components.

V. ADVANCED TMC TECHNIQUES

This section describes advanced TMC techniques not covered in the previous two sections.

A. SEMI-ACTIVE RECTIFIER WITH VARIABLE STRUCTURE

In Sections II and III, examples of static TMC were described. In those cases, some transistors operate in ON/OFF mode and switch an inverter or a rectifier circuit between different modes/topologies. However, there is also an active TMC when all transistors operate in the PWM mode, and the voltage gain of the converter is dependent on the PWM method. In the first example of the active TMC [55], a semi-active rectifier was demonstrated (see Fig. 29), which can operate as the VDR or the VQR depending on the switching patterns shown in Fig. 30. The circuit of the reconfigurable rectifier consists of two transistors, two diodes, and three capacitors. To balance voltage between the capacitors C_1 and C_2 in the VQR mode, the transistors operate sequentially one after the other: Q_1 is turned ON during one period, Q_2 is turned ON during the other period. The advantage of the rectifier with the active TMC is a lower component count than in the similar rectifier with the passive TMC from Section III-C.

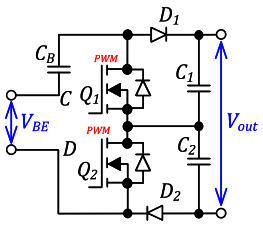

FIGURE 29. Active rectifier with variable structure.

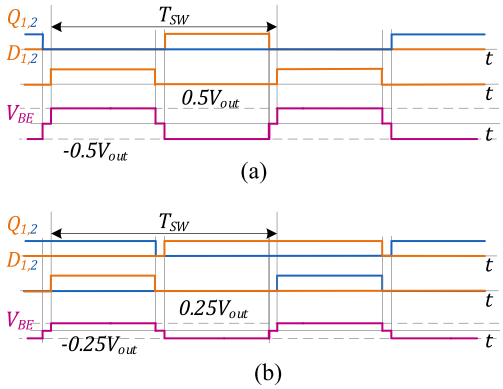

FIGURE 30. Operation of the semi-active rectifier as (a) VDR and (b) VQR.

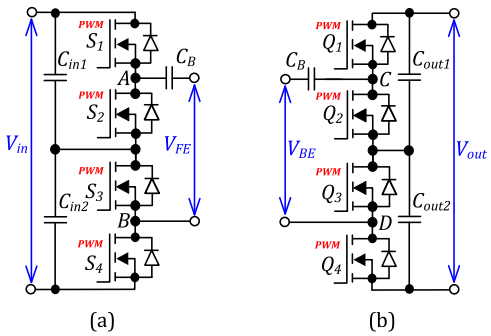

FIGURE 31. Active three-level half-bridge (a) inverter and (b) rectifier.

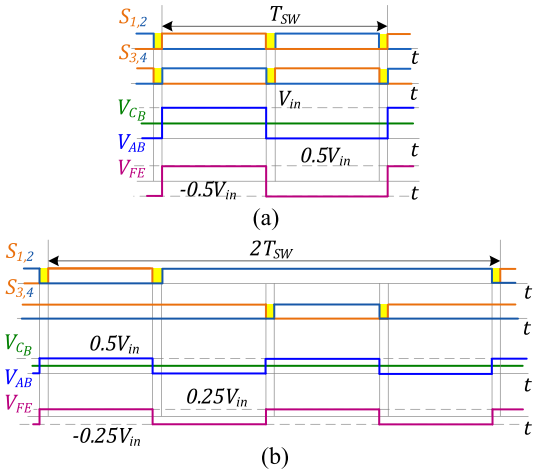

FIGURE 32. Operation of the active TL HBI inverter as (a) HBI and (b) QBI.

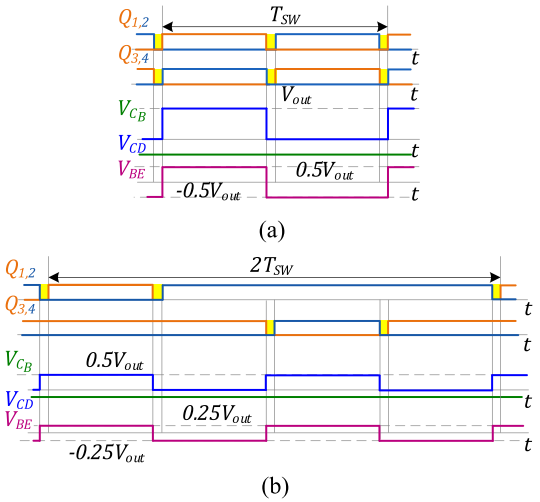

FIGURE 33. Operation of the active three-level half-bridge rectifier as the (a) VDR and the (b) VQR.

B. ACTIVE THREE-LEVEL HALF-BRIDGE INVERTER AND RECTIFIER WITH VARIABLE STRUCTURE

Another example of an active TMC is utilized for the three-level half-bridge inverter and rectifier, as shown in [56], [57], [58], [59]. Fig. 31 shows the topologies of the active TL HBI and the active TL HBR. The inverter and rectifier can operate in the HBI or the QBI mode, i.e., the VDR or the VQR mode, respectively. The circuits and operation principles of the inverter and the rectifier are similar. Therefore, only the operation of the inverter is described below. Half of the input voltage is applied to a transformer by turning ON the transistors S_1 and S_4 simultaneously (see Fig. 32(a)). The zero states in the switching cell are realized by turning ON switches S_2 and S_3. The QBI mode is realized by turning ON transistor pairs S_1 and S_3 or S_2 and S_4 (see Fig. 32(b)). To balance the voltage of the input capacitors C_{in1} and C_{in2} in the QBI mode, two pairs of transistors should be turned ON during equal time intervals. All inverter transistors are switched in this case, but the switching frequency is twice lower than that in the HBI mode. The voltage gain of the TL inverter G_{FE} equals 0.5 and 0.25 in the HBI mode and the QBI mode, respectively. The voltage gain of the TL rectifier G_{BE} equals 2 and 4 in the VDR and the VQR mode, respectively (see Fig. 33). The voltage stresses of the components in the inverter and rectifier equal half the voltage. The main disadvantage of the three-level half-bridge inverter and rectifier is the uneven current stress of the switches in the QBI and the VQR modes.

C. ADJUSTING THE TRANSFORMER TURNS RATIO

Another approach for extending the voltage gain of a converter is adjusting the turns ratio of a transformer by switching transformer tap windings. This simple approach has been applied in power engineering for a long time. The idea is to divide the output-side transformer windings into tapped sections and switch between them. Thus, the turns ratio of

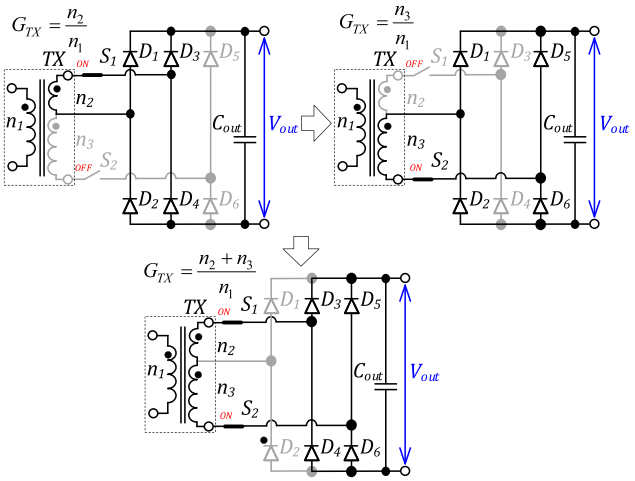

FIGURE 34. Reconfiguration of the transformer with two secondary windings.

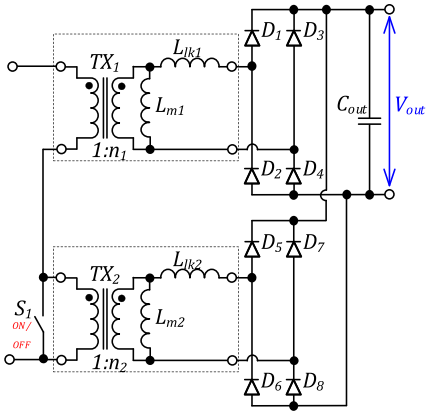

FIGURE 35. Reconfigurable topology with an enabled series transformer.

the transformer can be adjusted. As described in [60] and [61], this approach can also be applied to galvanically isolated dc-dc converters. Bidirectional switches enable or disable secondary windings and connect them to the three-leg full-bridge rectifier. Depending on the states of the switches, the turns ratio of the transformer G_{TX} takes three values, as shown in Fig. 34. Using bidirectional switches is the main disadvantage of this approach since each switch consists of two MOSFETS connected in the back-to-back configuration. In the described circuit, two MOSFETS and two diodes conduct current in two configurations, and four MOSFETS and two diodes conduct current in the third configuration. As a result, the series resistance of the rectifier is higher than that of the conventional FBR. Also, these MOSFETS require isolated drivers, which complicates the control system.

D. BYPASSING A SERIES TRANSFORMER

Besides switching windings of a transformer, switching between parallel transformers or enabling series transformers can be used to extend the range of the dc voltage gain of a converter. Fig. 35 shows a converter with two series transformers and two parallel FBRs proposed in [62]. The bidirectional switch S_1 enables or bypasses the second transformer TX_2, depending on the state of the switch. When the S_1 is turned OFF, the primary windings of the transformers are connected in series. Thus, the total turns ratio of the two transformers equals

$$G_{TX} = \frac{n_1 \cdot n_2}{n_1 + n_2} \tag{4}$$

where n_1 and n_2 are the turns ratio of transformers TX_1 and TX_2, respectively. Thus, enabling the second transformer decreases the total turns ratio and redistributes voltage between two series primary windings. It reduces the flux density in the first transformer when the front-end inverter provides voltage above a certain threshold. This approach was applied to the LLC converter, where enabling the second transformer also increases the equivalent magnetizing inductance of the resonant tank and minimizes the magnetizing current. As a result, the dc voltage gain of the given LLC converter is extended more than two times. However, an obvious disadvantage of the proposed approach is the doubled number of transformers and rectifier diodes compared with the conventional LLC converter.

E. DOUBLE FULL-BRIDGE LLC CONVERTER BASED ON RECONFIGURABLE THREE-LEG INVERTER

Another TMC technique of switching parallel–series transformers is described in [63], [64], and [65]. The proposed converter consists of a three-leg FBI and FBR, and two parallel transformers and series capacitors, which form two resonant tanks (see Fig. 36). The three-leg inverter can operate as the double full-bridge (DFBI) and supply two transformers or operate as the FBI or the HBI while supplying only one of the transformers. In the FBI and the HBI modes, the converter operates like the conventional LLC converter based on one transformer. In the DFBI mode, both resonant tanks operate in parallel, and the total turns ratio of transformers is $G_{GX} = n_1 + n_2$ because the secondary windings of the transformers are connected in series. Thus, the proposed converter operates under three modes, which cover a wide range of voltage gain.

A similar approach is proposed in [66], [67], and [68]. These studies demonstrate the LLC converter based on the dual HBI (DHBI), which operates under two similar modes: the DHBI mode and the conventional HBI mode. The difference between the DFBI and the DHBI is that a capacitor leg replaces a switch leg.

The main drawback of the dual-bridge approach is the double number of components, which is the same as in the previous examples.

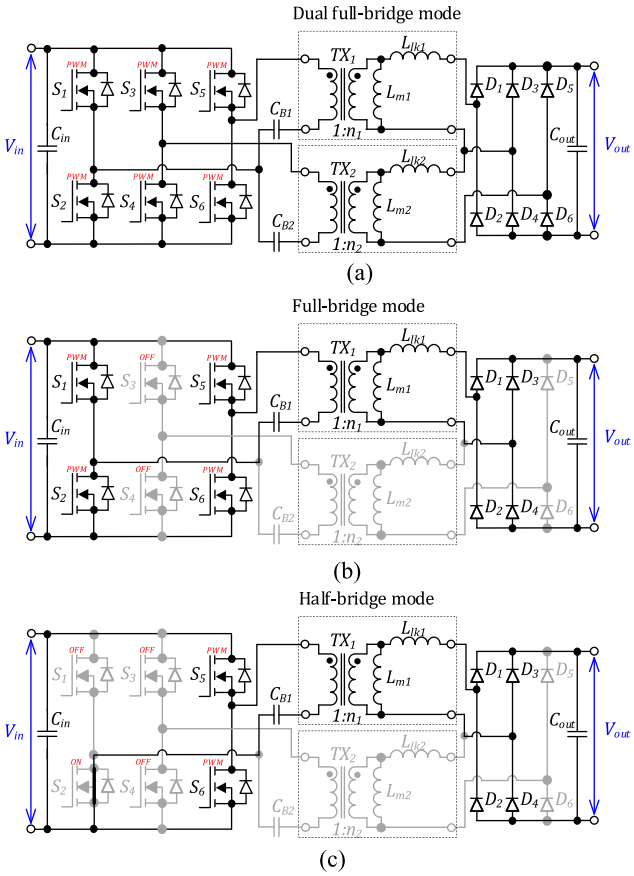

FIGURE 36. Reconfigurable double full-bridge LLC converter from the (a) DFBI to the (b) FBI and the (c) HBI.

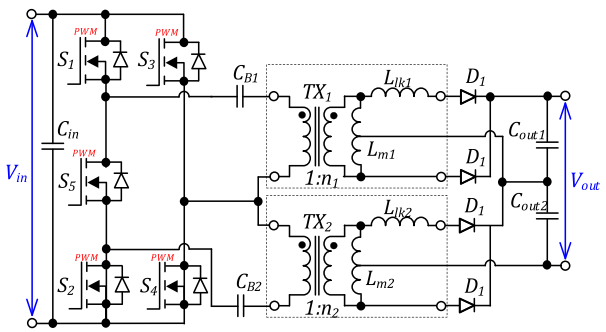

FIGURE 37. Five-switch bridge based reconfigurable converter.

F. FIVE-SWITCH RECONFIGURABLE INVERTER

Another TMC technique employing two transformers is presented in [69], [70], and [71]. Instead of the three-leg inverter, the five-switch bridge inverter (5H-inverter) is utilized along with two transformers. Both transformers are parts of parallel resonant converters, as shown in Fig. 37. The six operation modes of the 5H-inverter are shown in Fig. 38. Depending on the switching sequence, the first or/and second resonant converters operate with the HBI or the FBI. Theoretically, the same number of modes, i.e., equivalent topologies, is possible for the previous example. The main difference between the

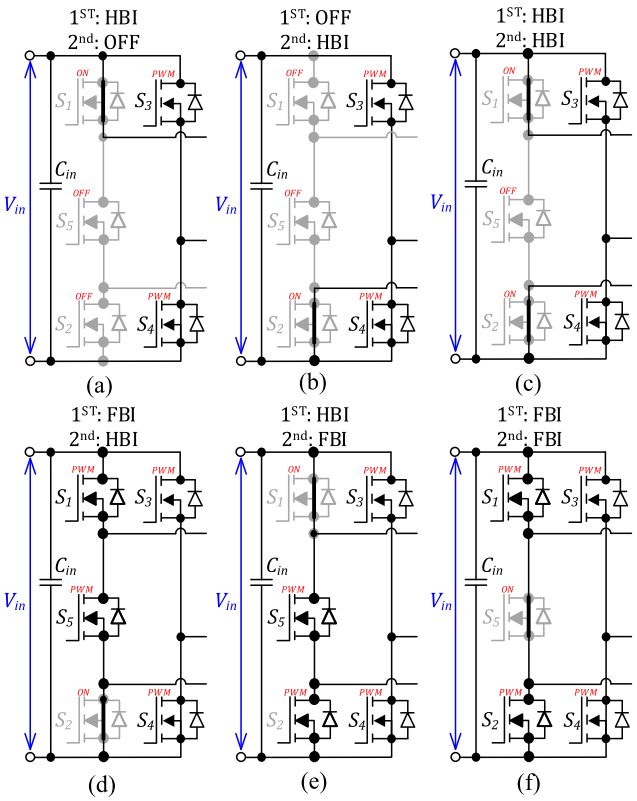

FIGURE 38. Operation modes of the 5H-inverter. (a) HBI / OFF. (b) OFF / HBI. (c) HBI / HBI. (d) FBI / HBI. (e) HBI / FBI. (f) FBI / FBI.

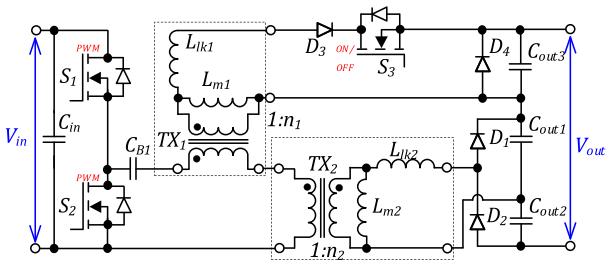

FIGURE 39. LLC converter with an auxiliary transformer and a half-wave rectifier.

DHBI and the 5H-inverter is in the number of switches: six against five.

G. LLC WITH AUXILIARY COUPLED INDUCTOR

In the TMC examples with two transformers described above, the rated power of the transformers in each converter is the same. However, converters with an auxiliary coupled inductor have been proposed in [72] and [73] to extend the voltage gain range of the resonant converters. The auxiliary coupled inductor is connected to a half-wave rectifier (HWR), which consists of diodes D_3 and D_4, and capacitor C_3 (see Fig. 39). When the bidirectional switch S_1 is disabled, the topology operates like the conventional LLC converter with the VDR. The magnetizing inductance of the coupled inductor TX_1 is part of the resonant tank. When the switch S_1 is enabled,

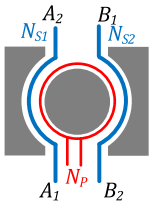

FIGURE 40. Transformer with secondary fractional turns.

the output voltage will be equal to the summed outputs of the HWR and VDR. The drawback of this approach is the power loss in the auxiliary coupled inductor even when the HWR is disabled because the resonant current flows through the primary winding of the inductor TX_1.

H. TRANSFORMERS WITH A FRACTIONAL TURNS RATIO

Another approach of TMC in the transformer stage is proposed in [74], [75], [76], and [77]. In their approach, a transformer with fractional turns ratio is utilized as an isolation transformer in the LLC converter. Dividing flux from the transformer turns allows for achieving a fractional turns ratio. It can be used in step-up/down applications with a high turns ratio for decreasing the number of turns. The proposed transformer has N_P total turns wound on the primary side and two secondary turns implemented from half turns (see Fig. 40). Each secondary half-turn is connected to an FBR through a blocking capacitor, as shown in Fig. 41.

Each rectifier can operate in the FBR, the HBR, or the zero mode. When both rectifiers operate in the FBR mode, the effective turns ratio of the converter equals N_P:0.5. The combination of operation modes in the rectifier gives four different effective turns ratios: N_P:0.5, N_P:2/3, N_P:1, N_P:2, achieved by combining FBR and FBR, FBR and HBR, HBR and HBR, and HBR and the zero modes, respectively. Implementation of the transformer with fractional turns requires a specific design. The examples described in the literature are based on planar cores with the printed circuit board (PCB) turns to optimize the size of converters. The PCB-based implementation could reduce the production cost of such converters. However, this TMC technique requires high semiconductor component count and associated circuitry.

On the other hand, an advanced planar transformer design along with an active TL HBI at the input and two active FBR cells at the output side resulted in the variable–inverter–rectifier–transformer concept [74]. It is the ultimate example of the TMC in the galvanically isolated dc-dc converters, providing numerous operating modes and, consequently, significantly extending the range of voltage gain regulation.

I. RECONFIGURABLE RESONANT TANK

Apart from controlling the resonant inductance and the equivalent turns ratio of transformers in the LLC converters, the TMC can be applied to the resonant tank. Studies in [78] and [79] describe modified resonant converters, where the LLC resonant tank could be reconfigured to the LLCC resonant tank. As can be seen from Fig. 42, a bidirectional switch controls the type of the resonant tank. When the switch is turned ON, the converter operates as the LLCC topology. When the switch is turned OFF, it operates like the conventional LLC topology. It allows for extending the voltage gain range while operating within a narrow switching frequency range. The described approach is one of the simple methods for extending the voltage gain range in the LLC converters.

J. MULTITRACK CONVERTER ARCHITECTURE

Another scalable and reconfigurable architecture of galvanically isolated dc-dc converters employing the TMC is presented in [80], [81]. Its simplest embodiment, the two-track converter, consists of the switched inductor (boost) circuit, hybrid double inverter, and isolation stage (with two transformers). The switched inductor circuit operates as the boost converter when the input voltage is less than V_X, where V_X and $2V_X$ are two related intermediate bus voltages, as shown in Fig. 43. When the input voltage is between V_X and $2V_X$, the switch S_3 is turned ON continuously and S_4 is turned OFF, while the switches S_1 and S_2 balance voltages of capacitors C_1 and C_2. The hybrid inverter consists of switches $S_{5\ldots8}$, capacitors $C_{1\ldots3}$, and blocking capacitors C_{B1} and C_{B2}. The inverter structure implies operation with a dual-primary-winding transformer or two parallel transformers. The proposed TMC technique is based on merging several typical converter stages. It allows for operating in a wide voltage gain range and optimizing current and voltage stress in the components. The simplest implementation of the multitrack architecture requires at least eight transistors, each with the galvanically isolated auxiliary supply for the driving circuit, which limits its use in practice.

K. SUMMARY

Table 3 compares advanced TMC techniques and demonstrates advantages, disadvantages, typical voltage and power for each technique. The nominal voltage gain value in the table takes into account the voltage gain of a converter at a nominal voltage. As can be observed, the given techniques all target the voltage gain range extension. There is a distinct group based on using multiple transformers and reconfiguring their connections. The flexibility of these techniques depends on the combination of their turns ratios, which are restricted by the regulation range of the original topology. Also, some of the advanced TMC techniques use very complex topologies that could be justified only for niche applications where the achieved flexibility could rationalize the cost of implementation.

VI. TMC IMPLEMENTATION EXAMPLES

This section focuses on the implementation of the TMC in practical applications.

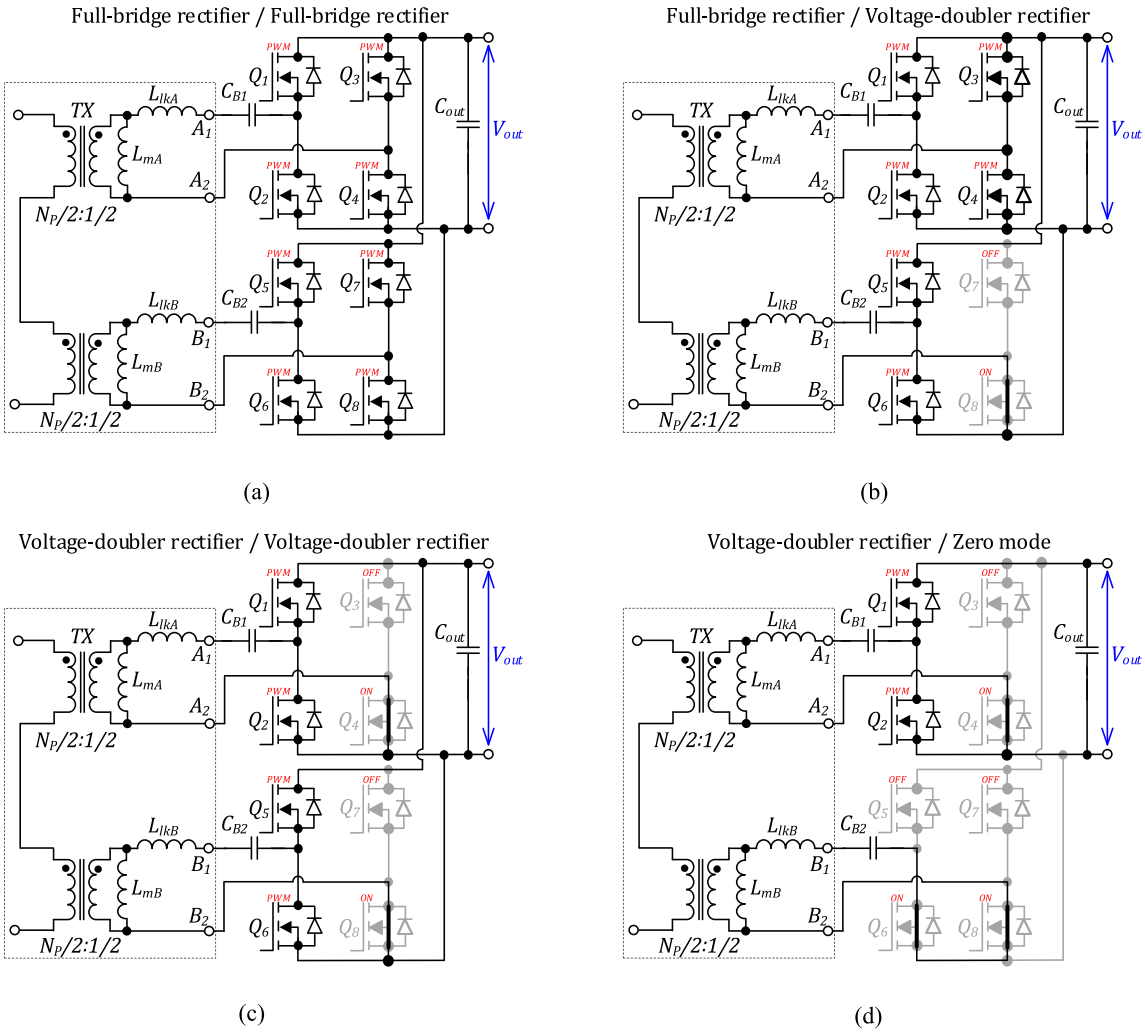

FIGURE 41. Reconfigurable LLC converter based on a transformer with fractional turns. (a) FBR / FBR, (b) FBR / VDR, (c) VDR / VDR, (d) and VDR / Zero mode.

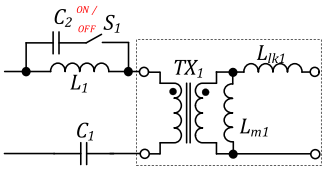

FIGURE 42. Reconfiguration from LLC to LLCC resonant tank.

A. FAULT-TOLERANT PV MICROCONVERTER

The TMC could be implemented for fault tolerance in a galvanically isolated high step-up photovoltaic (PV) microconverter. The study in [47] proposed a galvanically isolated dc-dc converter consisting of the quasi-Z-source network at the input, the FBI, an isolation transformer, and the reconfigurable rectifier with one active switch (see Fig. 44). To extend the input voltage range, the proposed microconverter can operate in the boost and buck modes. The PV microconverter can tolerate transistor faults in the FBI as the most stressed part of the microconverter. When a short-circuit failure (SCF) happens in one of the inverter switches, the inverter is reconfigured from the FBI to the SSI or the HBI in the boost mode or the buck mode, respectively, as shown in Fig. 45. At the same time, the rectifier is reconfigured from the FBR to the VDR in both modes. After the reconfiguration, the inverter changes the voltage gain from $G_{FE} = 1$ to $G_{FE} = 0.5$, and the rectifier changes the voltage gain from $G_{BE} = 1$ to $G_{BE} = 2$. Thus, the total dc voltage gain remains the same after the SCF and the microconverter can continue normal operation in the same voltage range.

B. SHADE-TOLERANT PV MICROCONVERTER

In the second example from paper [82], the TMC was utilized for extending an input voltage range of a PV microconverter to minimize power losses under the partial shading condition of a PV module. The proposed PV microconverter consists of the front-end quasi-Z-source SSI, an isolation transformer, and a reconfigurable rectifier, as shown in Fig. 46. Below a certain input voltage, the rectifier operates as the VQR. It is reconfigured into the VDR when the input voltage is above that

TABLE 3 Comparison of Advanced TMC Techniques

TMC	Nominal voltage gain G	Number of components[1]				Cost[3]	Advantage	Disadvantage	Typical input dc voltage, V	Typical output dc voltage, V	Typical power, W
		S	D	C	TX						
SAR (Fig. 29)	$2{\cdot}n$; $4{\cdot}n$	2	2	3	1	$	Voltage gain range extension up to two times	Switching losses in transistors	400	100–500	1500 [55]
A-TL FBI/ A-TL BBR (Fig. 31)	$0.5{\cdot}n$; $0.25{\cdot}n$ / $2{\cdot}n$; $4{\cdot}n$	4	0	3	1	$			400	50–450	300 [56], [57]
									160–280	18	100 [58]
									85–340	20	50 [59]
Adjusting turns ratio (Fig. 34)	n_1; n_2; $n_1{+}n_2$	8	6	1	1[2]	$$$	Voltage gain range extension depending on turns ratios	High number of semiconductor devices, using of bidirectional switches, using two transformers	390	250–450	1350 [60]
									390	60–450	900 [61]
Bypass. Series Transformer (Fig. 33)	n_1; $\frac{n_1 \cdot n_2}{n_1 + n_2}$	6	8	1	2	$$			25–100	210	250 [62]
Double LLC Conv. (Fig. 36)	n_1; n_2; $n_1{+}n_2$	6	6	4	2	$$		High number of semiconductor devices, using two transformers	50–300	50	250 [63]
									700	18–126	5000 [65]
									400	250–400	3200 [66]
									80–200	400	1000 [67]
									120–240	96	1000 [68]
5H-Inverter (Fig. 37)	$0.5n_1$; $0.5n_2$; $0.5n_1{+}0.5n_2$; $n_1{+}0.5n_2$; $0.5n_1{+}n_2$; $n_1{+}n_2$;	5	4	5	2	$$		Using two transformers	390	100–420	1100 [69]
									390	80–450	1000 [70]
									320–420	55–420	1000 [71]
LLC with Auxiliary Coupled Inductor (Fig. 39)	n_1; $n_1{+}n_2$	3	4	5	2	$$			5–65	400	400 [72]
									22–40	400	240 [73]
Fractional Turns Ratio (Fig 41)	$n_P{:}0.5$, $n_P{:}2/3$, $n_P{:}1$, $n_P{:}2$,	12	0	4	1[2]	$$$	Voltage gain range extension up to four times	Complex design of a transformer, high number of transistors	120–380	5, 9, 12	36 [74]
									380	12	1000 [75]
									250–500	10.5–15	1000 [77]
Reconfig. Resonant Tank (Fig. 42)	n; $2.5{\cdot}n$	6	4	4	1	$	Voltage gain range extension up to 2.5 times	Using of a bidirectional switch	150–400	400	1000 [78]
									140–400	400	1000 [79]
Multi-Track Architecture (Fig. 43)	$0.5\ n$; n	8	4	6; L=1	1[2]	$$$	Voltage gain range extension up to two times	High number of components	18–80	5	75 [80]
									80–370	12	150 [81]

Note: [1]S=switch; D=diode; C=capacitor; L=inductor, TX=transformer;
[2]A transformer with two primary or secondary windings.
[3]Estimated cost: $ is a low cost; $$ is a medium cost; $$$ is a high cost.

threshold value. The rectifier operation modes are selected by switching a mode-changing switch Q_1, which operates in the ON/OFF mode. Thus, high performance was achieved in the input voltage range from 8 up to 50 V, despite the simplified front-end inverter utilizing fewer switches. This range enables the maximum power point tracking under different partial shading conditions of the widespread 60-cell Si-based PV modules.

C. PV MICROCONVERTER WITH FLAT EFFICIENCY CURVE

TMC is also applied in PV microconverters for efficiency flattening across a power range [32]. The given PV microconverter consists of the FBI and the active FBR, as shown in Fig. 47; the aim is to achieve bidirectional power flow for possible battery integration. The idea presented in the article is based on the reconfiguration of the FBI to the flyback converter and the FBR to the SSR at a light load (see Fig. 48). According to the study, applying this reconfiguration at loads below 40% allows for improving the efficiency by up to 8%. The main drawback of the proposed approach is the requirement for using one bidirectional switch in the rectifier for blocking one leg in the SSR mode. It increases the cost of the rectifier and conducting losses in the FBR mode compared to the conventional FBR. Moreover, this approach is useful in low-power applications as the transformer air gap shall be large enough to handle power transfer in the flyback mode, which increases the conduction losses from the magnetizing current in the FBI mode.

D. UNIVERSAL HIGH STEP-UP INTERFACE CONVERTER FOR DC MICROGRIDS

Another example of TMC application that allows for a wide input voltage range and flattened efficiency curve is presented

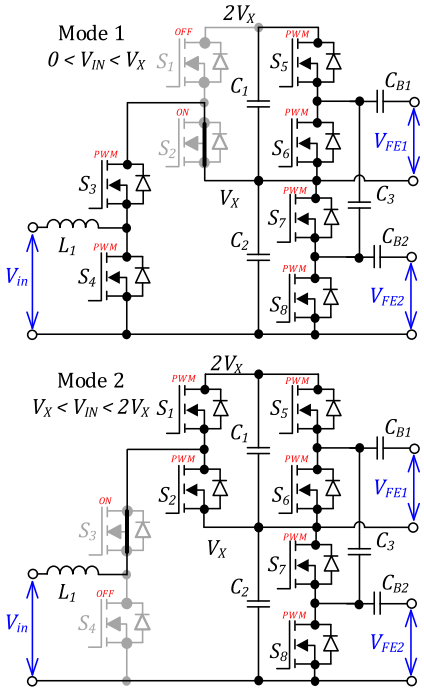

FIGURE 43. Operation modes of the two-track converter.

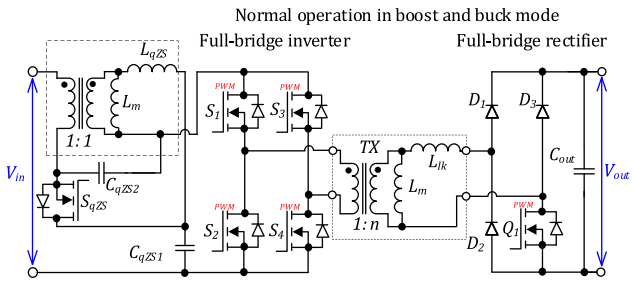

FIGURE 44. Quasi-Z-source galvanically isolated PV microconverter.

in [83]. In that study, the bidirectional isolated hexa-mode dc-dc converter (IHMC) based on the SRC topology is presented. The converter has a symmetrical structure that utilizes hybrid FBI cells both at the input and output sides. Each hybrid switching cell can operate as the FBI or the HBI. Thus, the IHMC operates under three topology configurations in each power flow direction: the FBI-FBR, the HBI-FBR, and the FBI-VDR (see Fig. 49).

In each mode, the converter operates as a buck-boost converter with the synchronous rectification. A special modulation is applied at the input side to step down the input voltage by reducing the active state duration at the isolation transformer, thus lowering the power throughput of the resonant tank. Similarly, using a special modulation at the output side allows for the input voltage boosting by short-circuiting the secondary winding with the resonant inductor, using the latter as an ac boost inductor. The TMC in this example provides for achieving a wide input voltage range from 10 to 60 V with an efficiency higher than 92% and the peak efficiency of 98%.

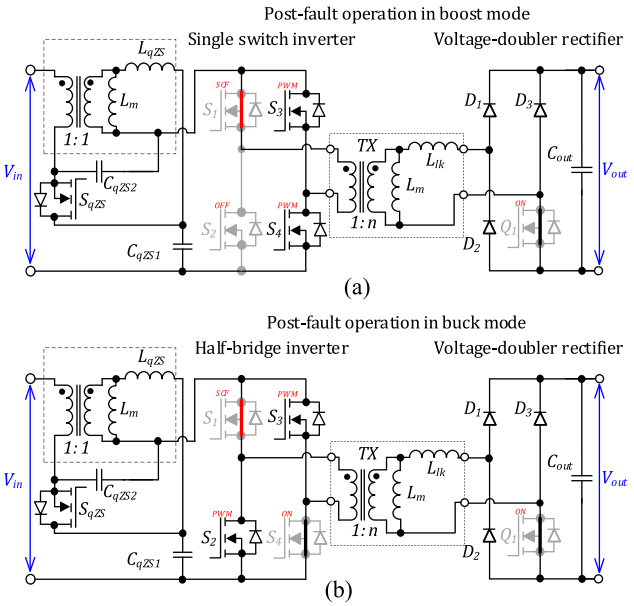

FIGURE 45. Post-fault operation of the quasi-Z-source galvanically isolated PV microconverter in the (a) boost and (b) buck modes.

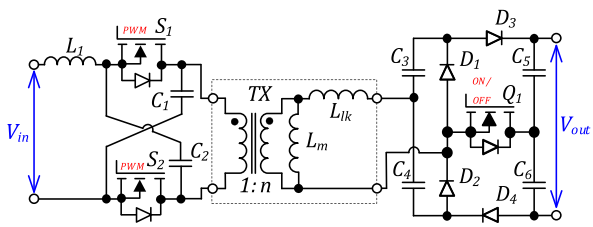

FIGURE 46. PV microconverter with a reconfigurable rectifier.

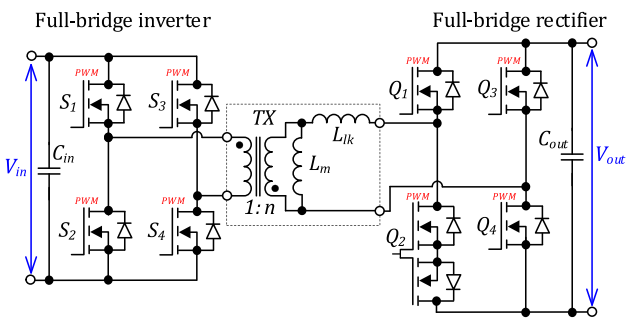

FIGURE 47. Dual-active bridge converter with flattened efficiency curve.

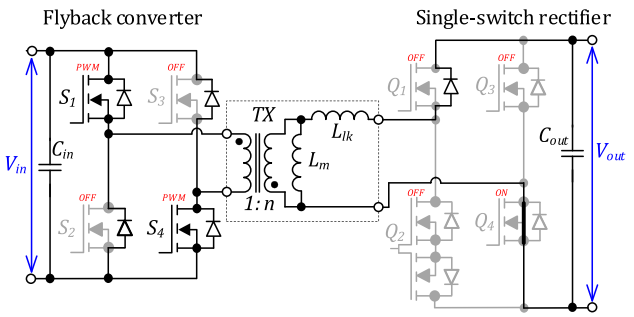

FIGURE 48. PV microconverter reconfiguration to the flyback converter at a light load.

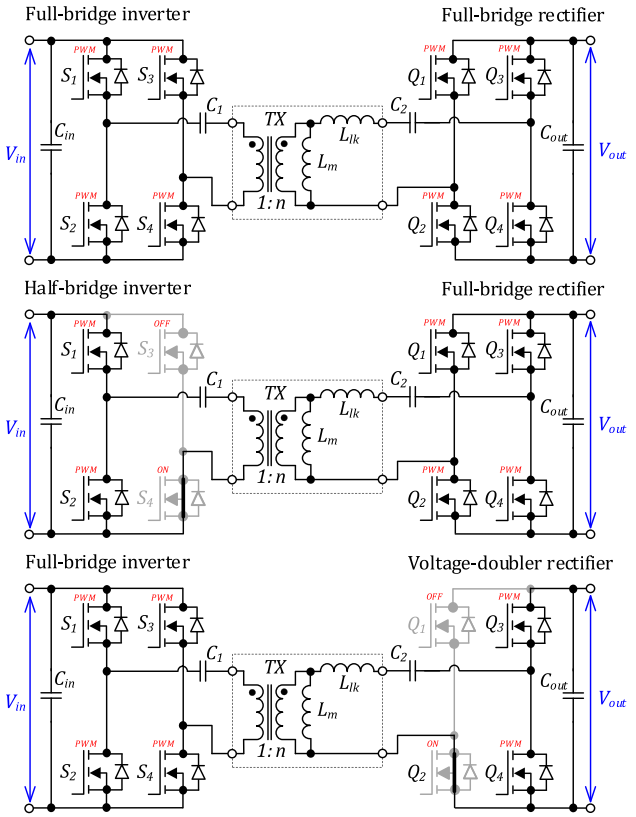

FIGURE 49. Operation modes of the galvanically isolated bidirectional hexa-mode dc-dc converter.

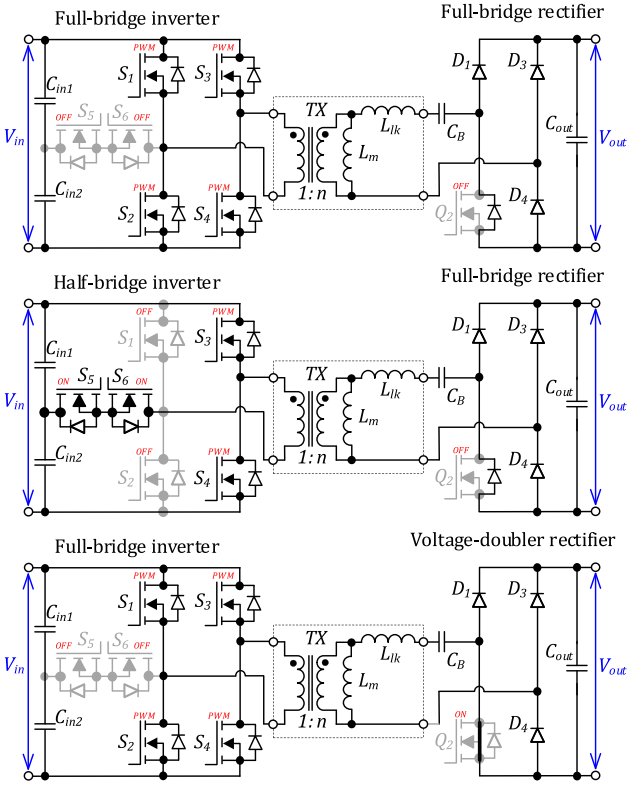

FIGURE 50. Operation modes of a universal PV microconverter.

E. MICROCONVERTER WITH DUAL-STANDARD OUTPUT VOLTAGE FOR PV APPLICATIONS

TMC was also used in a PV microconverter for operation with two different voltage levels of a dc link, such as 200 and 400 V. This makes the microconverter compatible with inverters operating at different ac voltage levels: 110/120 V and 220/230/240 V, extending their applicability in different geographic locations. As a solution, a universal PV microconverter is proposed in [21], in which the FBI can be reconfigured in the HBI, and the FBR can operate as the VDR (see Fig. 50).

The converter has three topology configurations: HBI-FBR, FBI-FBR, and FBI-VDR. The maximum normalized voltage gain of the converter in these modes equals $G = 0.5$, 1, and 2, respectively. Reconfiguration of the rectifier is applied for operation at different output voltage levels. At the same time, the inverter can operate in the FBI or the HBI mode. In the study, a hybrid mode for controlling the inverter was applied. During the active states, the inverter operates as the FBI. During the zero states, the inverter is reconfigured to the HBI to levelize the peak transformer magnetizing current and avoid incomplete zero-voltage switchings. Thus, the proposed converter operates with efficiency of up to 96% at the input voltage range from 30 to 60 V, and two output voltage levels of 200 and 400 V.

F. TELECOM BACKUP POWER SUPPLY WITH DUAL-STANDARD OUTPUT VOLTAGE

One more example of TMC application in this section exhibits an LLC converter for supplying telecom systems from a battery with a wide voltage range [19]. The proposed converter is designed for a 100–400 V input voltage, a 48/24 V output voltage, and a maximum power of 800 W. The wide input voltage range was achieved by applying the TMC in the front-end inverter, as shown in Fig. 51. In the input voltage range of 100–240 V, the front-end inverter operates in the FBI mode. In the input voltage range of 240–400 V, it switches to operation in the HBI mode. Thus, the TMC allows for achieving efficiency above 90% in the wide input voltage range. The study describes also a method for soft transition between modes and stabilization of the output voltage. However, the mode reconfiguration transitions limit the converter feasibility in applications with tight voltage regulation.

G. ELECTRIC VEHICLE CHARGER WITH A WIDE OUTPUT VOLTAGE RANGE

A good example of advanced TMC techniques is the electric vehicle charger presented in [69]. It utilizes a five-switch reconfigurable bridge with two transformers shown in Fig. 37. The authors demonstrate how this topology can interchange its normalized dc voltage gain between 1, 2, 3, and 4. It was verified using a 1.1 kW protype fed with 390 V input voltage. Using TMC, it achieves a fourfold output voltage range from 100 to 420 V. This converter not only outperforms

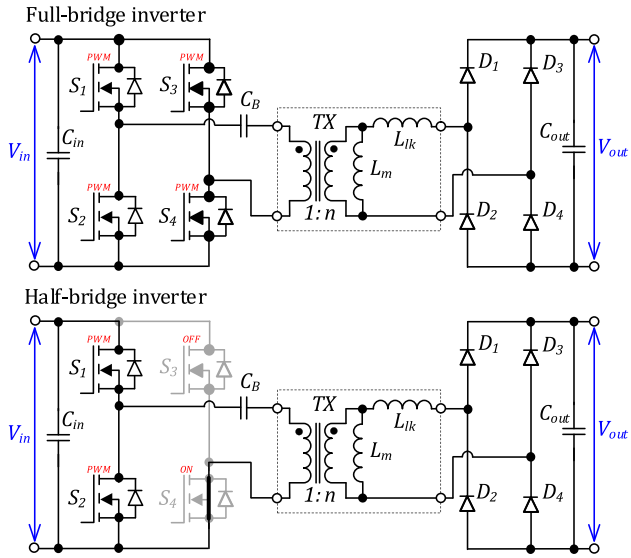

FIGURE 51. Reconfigurable LLC converter with wide input voltage range for the telecom system.

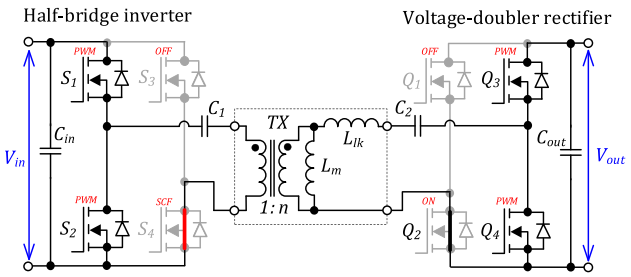

FIGURE 52. Post-fault operation of the dual active bridge converter.

the reference LLC converter-based chargers, but also features a narrow frequency regulation range. Owing to the use of TMC, it maintains its efficiency over 96% across the output voltage range and achieves the peak efficiency of 97.6%. Its obvious disadvantages are uneven thermal loading of the switches throughout the output voltage regulation range and overall complexity, which, however, could be acceptable for the applications where different standards require a very wide output voltage range from the chargers.

H. FAULT-TOLERANT CONVERTER FOR MORE ELECTRIC AIRCRAFTS

In more electric aircrafts, dc distribution is based on the use of two dc buses: 28 and 270 V. A converter interlinking them is required, where the dual active bridge is a common choice. In such a mission-critical system, a switch fault can occur, but it must not result in converter failure. For example, at an SCF in the switch S_4, the dual active bridge converter can continue operation as a dual half-bridge converter, as shown in Fig. 52. It is essential to mention that this converter could provide fault tolerance with zero redundancy, i.e., no redundant components. There are following two possible implementations of the converter:

1) conventional with a large inductor L_{lk} and phase shift modulation;
2) series-resonant implementation with a small L_{lk} that is likely to be embedded into the transformer *TX*.

It could be shown that zero-redundancy post-fault operation of the conventional implementation is not feasible due to the low power throughput of the post-fault dual half-bridge converter, which is four times lower than that before a fault.

On the other hand, the resonant implementation can handle post-fault operation at the same switching frequency. It can match the low-voltage port range from 18 to 50 V and the high-voltage port range from 200 to 330 V [84]. Pre-fault efficiency of a 300 W prototype ranges from 91% to 97.8%. The post-fault efficiency values ranging from 86% to 96% result from much increased current stress of the remaining healthy components.

VII. DISCUSSION

A. GENERALIZATION

Most of the TMC techniques could be summarized in the following basic principles: reducing voltage or current stress of semiconductors in a wide voltage range operation by reconfiguring the topology; reducing the number of switching components to improve light-load efficiency; recovering converter gain after a semiconductor fault; increasing converter dc gain at the output side to enable input side operation in a wider voltage range, while keeping the input-side duty cycle in an optimal range. It is worth mentioning that TMC has not shown power density improvement of the baseline converters. In some cases, power density could even be reduced due to specific thermal design requirements or the complicated design of magnetic components. On the other hand, the TMC enables single-stage high-performance dc-dc converters that could be smaller than the typical two-stage converter with the same functionality.

Several generalizations could be drawn from the literature surveyed in this article. Galvanically isolated dc-dc converters with low dc gain changing in a relatively wide range are typically designed for applications from several kW and higher, like on-board EV charging. Their implementation with LLC or series resonant switching with TMC on the input side could be recommended in the case of the wide input voltage range, or TMC on the output side in the case of the wide output voltage range to keep the stress of semiconductor components constrained. Most of these applications would not require more than two-mode TMC techniques. TMC techniques based on three-level topologies would be helpful when the voltage range spans to voltages above the voltage blocking capability of generic semiconductor switches.

Applications with high dc gain typically deal with low power, often below a kilowatt. As a result, the front-end inverter is often rated for high current stress, leading to considerable input voltage and power efficiency variations. These efficiency variations could result in significant efficiency steps, i.e., thermal cycling, when a converter changes

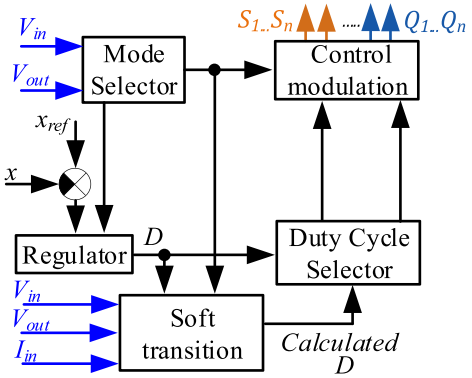

FIGURE 53. Example of TMC control integrated into a close-loop control system.

its operation mode based on TMC. However, the best-in-class dc gain range with no efficiency steps at the mode changes was observed in the converter combining boost half-bridge with reconfigurable rectifier [50]. Research efforts are required to determine whether this issue could be resolved for the full-bridge circuits.

Only a handful of techniques target efficiency improvement at light loads. These techniques have been used for low-power applications where reducing the number of active semiconductor devices at a light load could be very effective. At the same time, asymmetrical requirements for heat dissipation of devices are easy to manage in these applications. Nevertheless, some TMC techniques, such as reconfiguring FBI into HBI for better efficiency at a light load, could be useful in medium and high-power applications [85].

In addition, many advanced techniques resulting in high complexity of the converter design have been demonstrated for applications with high dc gain changing in a wide range. Their use can be recommended in niche applications, where strict performance requirements could justify associated extra costs.

B. CHALLENGES

Application of TMC techniques is challenging. First, the integration of TMC into a control system of a converter requires an additional control loop for reconfiguring a topology depending on the input and output voltage or power. In addition, the parameters of a regulator in the control system should be changed with topology reconfiguration due to changes in the small-signal converter model for each topology configuration. An example of a control system is shown in Fig. 53. The mode selector block changes topology configuration when voltage gain changes and crosses a threshold. With changing topology configuration, the mode selector also changes the parameters of the regulator.

The second challenge in control is the implementation of transitions between topology configurations with stabilized input and output voltage and current. Hard transitions between configurations cause high current stress in components that can damage a converter. Few studies have presented soft-transition algorithms [19], [86]. During the soft transition, the control system disables a regulator and sets a precalculated value for control variable D. Subsequently, the control system switches back to normal operation.

An efficiency step change that happens after a transition between topology configurations can be highlighted as the third challenge. The efficiency step change results in a considerable difference in power losses after the transition. Therefore, when the converter crosses the transition point, the temperature of the converter components changes. It would result in accelerated degradation of the converter components. To minimize the thermal stress of the components, the converter should be designed to map the mode transition points away from the most probable operation voltages or currents, if possible. Moreover, the thermal design of the converter should be based on the worst-case analysis of losses in each component for different modes.

C. PROMISING APPLICATIONS

As our review of the literature shows, the TMC is becoming more popular in applications with a wide input or output voltage range, such as chargers or battery interfaces. This trend suggests that TMC will gain even more attention in connection with the development of new portable electronic devices, electric scooters and bicycles [87]. In addition, the accelerating adoption of battery energy storage systems could benefit from the use of more flexible power electronic interface converters [88], [89].

The second expected trend is power electronics for supplying new USB Power Delivery (PD) specification (revision 3.1) that allows for delivery of up to 240 W over the USB type-C interface. USB fast chargers are expected to become a ubiquitous solution for portable electronics. The TMC could be a solution for the realization of efficient chargers capable of providing all output voltages requested by the USB PD specification (5, 9, 12, 20, 28, 36, and 48 V) [90].

The other promising application field for the TMC is fast chargers and on-board chargers for electrical vehicles (EV) and hybrid plug-in vehicles due to a wide voltage range of on-board batteries. The battery voltage standard has increased from 400 to 800 V [91]. Predictably, higher battery voltages allow for decreasing conduction losses in EVs. The TMC enables new chargers with a wide output voltage range.

Besides EVs, more electrical aircrafts could become a priority application area for the TMC [92], [93]. TMC increases the efficiency of converters operating in a wide range of on-board dc bus voltages and enables low-cost implementation of fault tolerance [84].

DC-microgrids for residential and small commercial buildings are becoming more popular due to their high efficiency compared to the ac grid [94], [95]. A variety of residential solar photovoltaic modules and battery types for energy storage requires numerous application-specific interface converters. The TMC can also enable a new class of universal interface converters to integrate renewable energy sources into the dc

microgrids with a minimum number of stock keeping unit types [50].

Residential PV systems suffering from partial shading of PV modules need interface converters capable of global maximum power point tracking [96]. This feature requires those converters to ensure a wide input voltage range that could be achieved at a low cost using TMC [82].

Fuel cells have been under the spotlight due to recent governmental support to cleantech. Their application requires the development of dc-dc converters capable of wide input voltage range regulation and delivering the maximum power at the maximum dc gain [97], [98]. TMC could help to optimize current stress in components for this challenging application, but more studies focusing on application of TMC are needed to show all possible benefits [34].

D. PROTECTED INTELLECTUAL PROPERTY

It is important to mention that a number of TMC techniques identified are protected by patents by companies and inventors from academia.

Several designs were patented by ShanghaiTech University: TMC with two secondary windings (see Fig. 34) [99], 5H-inverter (see Fig. 38) [100], and reconfigurable rectifier from Fig. 25 [101].

Delta Electronics holds several patents for TMC techniques applied on the converter input side: TMC based on TL HBI (see Fig. 31) [102], [103], and FBI/HBI reconfiguration in the front-end inverter (see Fig. 5) [29].

Murata Manufacturing Co. holds a patent describing the flying capacitor TL FBI capable of operating in the FBI mode with full voltage swing on the transformer and HBI mode with twice reduced voltage swing applied to the transformer [104]. This TMC technique could be considered a reduced subset of the technique shown in Fig. 13.

Huawei Digital Power Technologies also holds a patent that covers reconfiguration of both stages of a galvanically isolated dc-dc converter, where they demonstrate embodiments similar to TMC implementing FBR/VDR (see Fig. 15) and three-level half-bridge rectifier (see Fig. 31) [105], [106].

Shanghai Fengtian Electronics Co. holds a pending patent application describing two techniques for LLC resonant converter: FBI/HBI reconfiguration of the front-end inverter and hybrid modulation when one of the legs operating at three times reduced frequency [107].

The list of the TMC techniques protected by patents will get more comprehensive with time. Hence, it could be recommended to look out for possible patent infringements or limit the use of TMC techniques in commercial products to those published in the public domain.

VIII. CONCLUSION

This article has reviewed the present state-of-the-art in the topology morphing control for galvanically isolated dc-dc converters, covering the most recent contributions, implementation techniques, and application examples. It can be concluded that the topology morphing control is increasingly applied for extending the dc voltage gain range or flattening the efficiency of galvanically isolated dc-dc converters. The main principle of the TMC is in the reconfiguration of a converter topology depending on voltage or power conditions for operating with higher efficiency. The article provides a "one-stop" information source with comprehensive categorization of topology morphing control techniques for galvanically isolated dc-dc converters. Furthermore, the term "topology morphing control" has been established and justified for use in future publications.

This review divides the TMC into categories based on the converter side where the TMC is applied, such as the input and the output sides, an isolation transformer, or a resonant tank. In addition, advanced TMC techniques are described in a separate section. The described TMC application example shows that the prevalent dc-dc converter topologies utilizing the TMC are the resonant LLC or SRC. Both typically contain a series dc blocking capacitor allowing the use of the hybrid full-bridge switching cell that can easily be reconfigured from the full-bridge to the half-bridge. Most of the TMC techniques are based on static control of switches or the use of static switching patterns defining the operating mode. Hence, a simple control with smooth transitions between the modes is typically feasible. On the other hand, switching between TMC modes could result in a sizable efficiency step, which could have negative influence on the converter lifetime. This requires additional analysis with the focus on the minimization of mode transition instants, how to reduce efficiency steps at the mode transitions, and how these efficiency steps and their frequency influences the accumulated damage of components.

In conclusion, the application of the TMC gives a low-cost opportunity to improve converter performance, like increasing efficiency in a wide voltage gain range or a power range in galvanically isolated dc-dc converters. Publications on the subject have doubled in the past few years, revealing that there is still plenty of room for further development. Obviously, the proliferation of the dc nano- and microgrids, battery energy storage systems, and residential PV generation will create demand for high-performance low-cost converters and, consequently, will facilitate industrialization of the TMC.

REFERENCES

[1] M. Blonsky, A. Nagarajan, S. Ghosh, K. McKenna, S. Veda, and B. Kroposki, "Potential impacts of transportation and building electrification on the grid: A review of electrification projections and their effects on grid infrastructure, operation, and planning," *Curr. Sustain./Renewable Energy Rep.*, vol. 6, no. 4, pp. 169–176, Nov. 2019.

[2] European Commission, "Energy roadmap 2050-Impact assessment and scenario analysis," 2011. [Online]. Available: https://ec.europa.eu/energy/sites/ener/files/documents/roadmap2050_ia_20120430_en_0.pdf

[3] L. Mackay, N. H. van der Blij, L. Ramirez-Elizondo, and P. Bauer, "Toward the universal DC distribution system," *Elect. Power Compon. Syst.*, vol. 45, no. 10, pp. 1032–1042, Jun. 2017.

[4] T. Dragičević, X. Lu, J. C. Vasquez, and J. M. Guerrero, "DC microgrids—Part II: A review of power architectures, applications, and standardization issues," *IEEE Trans. Power Electron.*, vol. 31, no. 5, pp. 3528–3549, May 2016.

[5] L. Mackay, T. Hailu, L. Ramirez-Elizondo, and P. Bauer, "Towards a DC distribution system-opportunities and challenges," in *Proc. IEEE 1st Int. Conf. DC Microgrids*, 2015, pp. 215–220.

[6] M. Su, Z. Liu, Y. Sun, H. Han, and X. Hou, "Stability analysis and stabilization methods of DC microgrid with multiple parallel-connected DC-DC converters loaded by CPLs," *IEEE Trans. Smart Grid*, vol. 9, no. 1, pp. 132–142, Jan. 2018.

[7] V. A. K. Prabhala, B. P. Baddipadiga, and M. Ferdowsi, "DC distribution systems—An overview," in *Proc. Int. Conf. Renewable Energy Res. Appl.*, 2014, pp. 307–312.

[8] D. Tan, "Transportation electrification: Challenges and opportunities," *IEEE Power Electron. Mag.*, vol. 3, no. 2, pp. 50–52, Jun. 2016.

[9] R. Alexander, D. Meyer, and J. Wang, "A comparison of electric vehicle power systems to predict architectures, voltage levels, power requirements, and load characteristics of the future all-electric aircraft," in *Proc. IEEE Transp. Electrific. Conf. Expo.*, 2018, pp. 194–200.

[10] G. Buticchi, L. Costa, and M. Liserre, "Improving system efficiency for the more electric aircraft: A look at dc\/dc converters for the avionic onboard dc microgrid," *IEEE Ind. Electron. Mag.*, vol. 11, no. 3, pp. 26–36, Sep. 2017.

[11] E. Ragonese, N. Spina, A. Parisi, and G. Palmisano, "An experimental comparison of galvanically isolated DC-DC converters: Isolation technology and integration approach," *Electronics*, vol. 10, no. 10, May 2021, Art. no. 1186.

[12] A. Chub, D. Vinnikov, F. Blaabjerg, and F. Z. Peng, "A review of galvanically isolated impedance-source DC-DC converters," *IEEE Trans. Power Electron.*, vol. 31, no. 4, pp. 2808–2828, Apr. 2016.

[13] J. A. Ferreira and P. Wilson, "The impact of ITRW: How can WBG power semiconductors break through?," *IEEE Open J. Power Electron.*, vol. 2, pp. 327–335, 2021.

[14] J. M. Silveyra, E. Ferrara, D. L. Huber, and T. C. Monson, "Soft magnetic materials for a sustainable and electrified world," *Science*, vol. 362, Oct. 2018, Art. no. 6413.

[15] C. Jiang, X. Li, S. S. Ghosh, H. Zhao, Y. Shen, and T. Long, "Nanocrystalline powder cores for high-power high-frequency power electronics applications," *IEEE Trans. Power Electron.*, vol. 35, no. 10, pp. 10821–10830, Oct. 2020.

[16] D. Vinnikov, A. Chub, E. Liivik, and I. Roasto, "High-performance Quasi-z-source series resonant DC-DC converter for photovoltaic module-level power electronics applications," *IEEE Trans. Power Electron.*, vol. 32, no. 5, pp. 3634–3650, May 2017.

[17] Q. Xu, N. Vafamand, L. Chen, T. Dragičević, L. Xie, and F. Blaabjerg, "Review on advanced control technologies for bidirectional DC/DC converters in DC microgrids," *IEEE J. Emerg. Sel. Topics Power Electron.*, vol. 9, no. 2, pp. 1205–1221, Apr. 2021.

[18] M. M. Jovanović and B. T. Irving, "Efficiency optimization of LLC resonant converters operating in wide input- and/or output-voltage range by on-the-fly topology-morphing control," in *Proc. IEEE Appl. Power Electron. Conf. Expo.*, 2015, pp. 1420–1427.

[19] M. M. Jovanović and B. T. Irving, "On-the-fly topology-morphing control—Efficiency optimization method for LLC resonant converters operating in wide input- and/or output-voltage range," *IEEE Trans. Power Electron.*, vol. 31, no. 3, pp. 2596–2608, Mar. 2016.

[20] X. Sun, X. Li, Y. Shen, B. Wang, and X. Guo, "Dual-bridge LLC resonant converter with fixed-frequency PWM control for wide input applications," *IEEE Trans. Power Electron.*, vol. 32, no. 1, pp. 69–80, Jan. 2017.

[21] Y. Shen, H. Wang, A. Al-Durra, Z. Qin, and F. Blaabjerg, "A structure-reconfigurable series resonant DC-DC converter with wide-input and configurable-output voltages," *IEEE Trans. Ind. Appl.*, vol. 55, no. 2, pp. 1752–1764, Mar./Apr. 2019.

[22] G. Xu, D. Sha, Y. Xu, and X. Liao, "Hybrid-bridge-based DAB converter with voltage match control for wide voltage conversion gain application," *IEEE Trans. Power Electron.*, vol. 33, no. 2, pp. 1378–1388, Feb. 2018.

[23] Y. Wei and A. Mantooth, "A simple smooth mode transition strategy for resonant converters with topology morphing control in renewable energy applications," in *Proc. IEEE 4th Int. Conf. DC Microgrids*, 2021, pp. 1–7.

[24] Z. Liang, R. Guo, G. Wang, and A. Huang, "A new wide input range high efficiency photovoltaic inverter," in *Proc. IEEE Energy Convers. Congr. Expo.*, 2010, pp. 2937–2943.

[25] C. Loef and R. W. De Doncker, "An efficiency-optimized mode of operation for a resonant dc-dc converter with extended input voltage range for solar applications in dc-microgrids: Using topology-morphing to improve converter efficiency," in *Proc. IEEE 6th Int. Symp. Power Electron. Distrib. Gener. Syst.*, 2015, pp. 1–6.

[26] J. Wen, K. Sheng, J. Zhang, S. Yang, and W. Jiang, "A wide output LLC converter based on full bridge and half bridge topology morphing method using trajectory transition," in *Proc. IEEE Energy Convers. Congr. Expo.*, 2018, pp. 6817–6821.

[27] L. Costa, G. Buticchi, and M. Liserre, "A fault-tolerant series-resonant DC-DC converter," *IEEE Trans. Power Electron.*, vol. 32, no. 2, pp. 900–905, Feb. 2017.

[28] M. Abbasi, R. E. Shalkouhi, K. Kanathipan, M. A. M. Cheema, and J. Lam, "A step-up reconfigurable multi-mode LLC converter module with extended high efficiency range for wide voltage gain application in medium voltage DC grid systems," *IEEE Trans. Power Electron.*, vol. 37, no. 7, pp. 8118–8132, Jul. 2022.

[29] M. M. Jovanovic and B. T. Irving, "Power converters for wide input or output voltage range and control methods thereof," U.S. Patent 9263960B2, Feb. 16, 2016.

[30] V. Sidorov, A. Chub, D. Vinnikov, and A. Bakeer, "An overview and comprehensive comparative evaluation of constant-frequency voltage buck control methods for series resonant DC-DC converters," *IEEE Open J. Ind. Electron. Soc.*, vol. 2, pp. 65–79, Jan. 2021.

[31] J. Kan, Y. Wu, Y. Tang, and S. Xie, " Flexible topology converter used in photovoltaic micro-inverter for higher weighted-efficiency," *IET Power Electron.*, vol. 12, no. 9, pp. 2361–2371, Aug. 2019.

[32] S. Poshtkouhi and O. Trescases, "Flyback mode for improved low-power efficiency in the dual-active-bridge converter for bidirectional PV microinverters with integrated storage," *IEEE Trans. Ind. Appl.*, vol. 51, no. 4, pp. 3316–3324, Jul./Aug. 2015.

[33] A. Chub, D. Vinnikov, R. Kosenko, and E. Liivik, "Wide input voltage range photovoltaic microconverter with reconfigurable buck-boost switching stage," *IEEE Trans. Ind. Electron.*, vol. 64, no. 7, pp. 5974–5983, Jul. 2017.

[34] K. Jin and X. Ruan, "Hybrid full-bridge three-level LLC resonant converter- A novel DC-DC converter suitable for fuel cell power system," in *Proc. IEEE 36th Power Electron. Spec. Conf.*, 2005, pp. 361–367.

[35] T. Jiang, J. Zhang, X. Wu, K. Sheng, and Y. Wang, "A bidirectional three-level LLC resonant converter with PWAM control," *IEEE Trans. Power Electron.*, vol. 31, no. 3, pp. 2213–2225, Mar. 2016.

[36] H. Haga and F. Kurokawa, "Modulation method of a full-bridge three-level LLC resonant converter for battery charger of electrical vehicles," *IEEE Trans. Power Electron.*, vol. 32, no. 4, pp. 2498–2507, Apr. 2017.

[37] W. Chen and X. Ruan, "Zero-voltage-switching PWM hybrid full-bridge three-level converter with secondary-voltage clamping scheme," *IEEE Trans. Ind. Electron.*, vol. 55, no. 2, pp. 644–654, Feb. 2008.

[38] F. Canales, T. H. Li, and D. Aggeler, "Novel modulation method of a three-level isolated full-bridge LLC resonant DC-DC converter for wide-output voltage application," in *Proc. 15th Int. Power Electron. Motion Control Conf.*, 2012, pp. DS2b.11–1–DS2b.11–7.

[39] Y. Xuan, X. Yang, W. Chen, T. Liu, and X. Hao, "A novel NPC dual-active-bridge converter with blocking capacitor for energy storage system," *IEEE Trans. Power Electron.*, vol. 34, no. 11, pp. 10635–10649, Nov. 2019.

[40] Y. Xuan, X. Yang, W. Chen, T. Liu, and X. Hao, "A novel three-level CLLC resonant DC-DC converter for bidirectional EV charger in DC microgrids," *IEEE Trans. Ind. Electron.*, vol. 68, no. 3, pp. 2334–2344, Mar. 2021.

[41] D. Shu and H. Wang, "Light-load performance enhancement technique for LLC-based PEV charger through circuit reconfiguration," *IEEE Trans. Transp. Electrific.*, vol. 7, no. 4, pp. 2104–2113, Dec. 2021.

[42] Y. Shen, H. Wang, Z. Shen, Y. Yang, and F. Blaabjerg, "A 1-MHz series resonant DC-DC converter with a dual-mode rectifier for PV microinverters," *IEEE Trans. Power Electron.*, vol. 34, no. 7, pp. 6544–6564, Jul. 2019.

[43] M. I. Shahzad, S. Iqbal, and S. Taib, "A wide output range HB-2LLC resonant converter with hybrid rectifier for PEV battery charging," *IEEE Trans. Transp. Electrific.*, vol. 3, no. 2, pp. 520–531, Jun. 2017.

[44] H. Higa, S. Takuma, K. Orikawa, and J. Itoh, "Dual active bridge DC-DC converter using both full and half bridge topologies to achieve high efficiency for wide load," in *Proc. IEEE Energy Convers. Congr. Expo.*, 2015, pp. 6344–6351.

[45] A. Kumar, J. Lu, and K. K. Afridi, "Power density and efficiency enhancement in ICN DC-DC converters using topology morphing control," *IEEE Trans. Power Electron.*, vol. 34, no. 2, pp. 1881–1900, Feb. 2019.

[46] J. -W. Kim and P. Barbosa, "PWM-controlled series resonant converter for universal electric vehicle charger," *IEEE Trans. Power Electron.*, vol. 36, no. 12, pp. 13578–13588, Dec. 2021.

[47] D. Vinnikov, A. Chub, D. Zinchenko, V. Sidorov, M. Malinowski, and S. Bayhan, "Topology-morphing photovoltaic microconverter with wide MPPT voltage window and post-fault operation capability," *IEEE Access*, vol. 8, pp. 153941–153955, 2020.

[48] M. Shang and H. Wang, "A voltage quadrupler rectifier based pulsewidth modulated LLC converter with wide output range," *IEEE Trans. Ind. Appl.*, vol. 54, no. 6, pp. 6159–6168, Nov./Dec. 2018.

[49] M. Abbasi, R. Emamalipour, M. A. Masood Cheema, and J. Lam, "An interchangeable soft-switched voltage boosting circuit for a multi-mode LLC step-up converter module in medium voltage applications," in *Proc. IEEE Energy Convers. Congr. Expo.*, 2020, pp. 393–398.

[50] A. Chub, D. Vinnikov, O. Korkh, M. Malinowski, and S. Kouro, "Ultrawide voltage gain range microconverter for integration of silicon and thin-film photovoltaic modules in DC microgrids," *IEEE Trans. Power Electron.*, vol. 36, no. 12, pp. 13763–13778, Dec. 2021.

[51] F. Alaql and I. Batarseh, "LLC resonant converter with reconfigurable voltage rectifier for wide input voltage applications," in *Proc. IEEE Energy Convers. Congr. Expo.*, 2020, pp. 1191–1196.

[52] M. Shang, H. Wang, and Q. Cao, "Reconfigurable LLC topology with squeezed frequency span for high-voltage bus-based photovoltaic systems," *IEEE Trans. Power Electron.*, vol. 33, no. 5, pp. 3688–3692, May 2018.

[53] A. Chub et al., "Wide-range operation of high step-up DC-DC converters with multimode rectifiers," *Electronics*, vol. 10, no. 8, Mar. 2021, Art. no. 914.

[54] S. Rivera, S. Kouro, S. Vazquez, S. M. Goetz, R. Lizana, and E. Romero-Cadaval, "Electric vehicle charging infrastructure: From grid to battery," *IEEE Ind. Electron. Mag.*, vol. 15, no. 2, pp. 37–51, Jun. 2021.

[55] H. Wu, Y. Li, and Y. Xing, "LLC resonant converter with semi-active variable-structure rectifier (SA-VSR) for wide output voltage range application," *IEEE Trans. Power Electron.*, vol. 31, no. 5, pp. 3389–3394, May 2016.

[56] Y. Zuo, X. Pan, and C. Wang, "A reconfigurable bidirectional isolated LLC resonant converter for ultra-wide voltage-gain range applications," *IEEE Trans. Ind. Electron.*, vol. 69, no. 6, pp. 5713–5723, Jun. 2022.

[57] L. Gu, W. Liang, M. Praglin, S. Chakraborty, and J. Rivas-Davila, "A wide-input-range high-efficiency step-down power factor correction converter using a variable frequency multiplier technique," *IEEE Trans. Power Electron.*, vol. 33, no. 11, pp. 9399–9411, Nov. 2018.

[58] Y. Wei, Q. Luo, and A. Mantooth, "Hybrid control strategy for LLC converter with reduced switching frequency range and circulating current for hold-up time operation," *IEEE Trans. Power Electron.*, vol. 36, no. 8, pp. 8600–8606, Aug. 2021.

[59] W. Inam, K. K. Afridi, and D. J. Perreault, "Variable frequency multiplier technique for high-efficiency conversion over a wide operating range," *IEEE J. Emerg. Sel. Topics Power Electron.*, vol. 4, no. 2, pp. 335–343, Jun. 2016.

[60] H. Wang, M. Shang, and D. Shu, "Design considerations of efficiency enhanced LLC PEV charger using reconfigurable transformer," *IEEE Trans. Veh. Technol.*, vol. 68, no. 9, pp. 8642–8651, Sep. 2019.

[61] D. Shu and H. Wang, "An ultrawide output range *LLC* resonant converter based on adjustable turns ratio transformer and reconfigurable bridge," *IEEE Trans. Ind. Electron.*, vol. 68, no. 8, pp. 7115–7124, Aug. 2021.

[62] H. Hu, X. Fang, F. Chen, Z. J. Shen, and I. Batarseh, "A modified high-efficiency *LLC* converter with two transformers for wide input-voltage range applications," *IEEE Trans. Power Electron.*, vol. 28, no. 4, pp. 1946–1960, Apr. 2013.

[63] Y. Wei, Q. Luo, and H. A. Mantooth, "An LLC converter with multiple operation modes for wide voltage gain range application," *IEEE Trans. Ind. Electron.*, vol. 68, no. 11, pp. 11111–11124, Nov. 2021.

[64] A. J. L. Joannou and D. Pentz, "Evaluation of a novel primary tapped transformer in a high frequency isolated power converter topology," in *Proc. IEEE Int. Conf. Ind. Technol.*, 2013, pp. 509–514.

[65] J. Oh et al., "A 3-bridge LLC resonant converter operating with a wide output voltage control range using morphing control for mode transitions," in *Proc. IEEE Appl. Power Electron. Conf. Expo.*, 2019, pp. 2300–2304.

[66] L. A. D. Ta, N. D. Dao, and D. Lee, "High-efficiency hybrid LLC resonant converter for on-board chargers of plug-in electric vehicles," *IEEE Trans. Power Electron.*, vol. 35, no. 8, pp. 8324–8334, Aug. 2020.

[67] W. Sun, Y. Xing, H. Wu, and J. Ding, "Modified high-efficiency LLC converters with two split resonant branches for wide input-voltage range applications," *IEEE Trans. Power Electron.*, vol. 33, no. 9, pp. 7867–7879, Sep. 2018.

[68] G. Xu, D. Sha, Y. Xu, and X. Liao, "Dual-Transformer-based DAB converter with wide ZVS range for wide voltage conversion gain application," *IEEE Trans. Ind. Electron.*, vol. 65, no. 4, pp. 3306–3316, Apr. 2018.

[69] C. Li, H. Wang, and M. Shang, "A five-switch bridge based reconfigurable LLC converter for deeply depleted PEV charging applications," *IEEE Trans. Power Electron.*, vol. 34, no. 5, pp. 4031–4035, May 2019.

[70] C. Li, M. Zhou, and H. Wang, "An H5-Bridge-based asymmetric LLC resonant converter with an ultrawide output voltage range," *IEEE Trans. Ind. Electron.*, vol. 67, no. 11, pp. 9503–9514, Nov. 2020.

[71] M. Zhou, D. Shu, and H. Wang, "An H5-Bridge-based laddered CLLC DCX with variable DC link for PEV charging applications," *IEEE Trans. Power Electron.*, vol. 37, no. 4, pp. 4249–4260, Apr. 2022.

[72] H. M. Maheri, D. Vinnikov, A. Chub, O. Korkh, A. Rosin, and E. Babaei, "Dual-mode magnetically integrated photovoltaic microconverter with adaptive mode change and global maximum power point tracking," *IET Renewable Power Gener.*, vol. 15, no. 1, pp. 86–98, Jan. 2021.

[73] Z. Liang, R. Guo, J. Li, and A. Q. Huang, "A high-efficiency PV module-integrated DC/DC converter for PV energy harvest in FREEDM systems," *IEEE Trans. Power Electron.*, vol. 26, no. 3, pp. 897–909, Mar. 2011.

[74] M. K. Ranjram, I. Moon, and D. J. Perreault, "Variable-inverter-rectifier-transformer: A hybrid electronic and magnetic structure enabling adjustable high step-down conversion ratios," *IEEE Trans. Power Electron.*, vol. 33, no. 8, pp. 6509–6525, Aug. 2018.

[75] M. K. Ranjram and D. J. Perreault, "A 380-12 V, 1-kW, 1-MHz converter using a miniaturized split-phase, fractional-turn planar transformer," *IEEE Trans. Power Electron.*, vol. 37, no. 2, pp. 1666–1681, Feb. 2022.

[76] Y.-C. Liu et al., "Design and implementation of a planar transformer with fractional turns for high power density LLC resonant converters," *IEEE Trans. Power Electron.*, vol. 36, no. 5, pp. 5191–5203, May 2021.

[77] J. D. Boles, S. Lim, J. A. Santiago-González, D. M. Otten, and D. J. Perreault, "A bidirectional LLC converter enabled by common-mode and differential-mode operation," in *Proc. IEEE Energy Convers. Congr. Expo.*, 2019, pp. 5116–5123.

[78] Y. Wang, R. Liu, F. Han, L. Yang, and Z. Meng, "Soft-switching DC-DC converter with controllable resonant tank featuring high efficiency and wide voltage gain range," *IET Power Electron.*, vol. 13, no. 3, pp. 495–504, Feb. 2020.

[79] R. M. Reddy, A. K. Jana, and M. Das, "Novel wide voltage range multi-resonant bidirectional DC-DC converter," in *Proc. IEEE Int. Conf. Power Electron., Drives Energy Syst.*, 2020, pp. 1–6.

[80] M. Chen, K. K. Afridi, S. Chakraborty, and D. J. Perreault, "Multitrack power conversion architecture," *IEEE Trans. Power Electron.*, vol. 32, no. 1, pp. 325–340, Jan. 2017.

[81] M. Chen, S. Chakraborty, and D. J. Perreault, "Multitrack power factor correction architecture," *IEEE Trans. Power Electron.*, vol. 34, no. 3, pp. 2454–2466, Mar. 2019.

[82] D. Vinnikov, A. Chub, O. Korkh, E. Liivik, F. Blaabjerg, and S. Kouro, "MPPT performance enhancement of low-cost PV microconverters," *Sol. Energy*, vol. 187, pp. 156–166, Jul. 2019.
[83] V. Sidorov, A. Chub, and D. Vinnikov, "Bidirectional isolated hexa-mode DC-DC converter," *IEEE Trans. Power Electron.*, vol. 37, no. 10, pp. 12264–12278, Oct. 2022.
[84] A. Chub, G. Buticchi, V. Sidorov, and D. Vinnikov, "Zero-redundancy fault-tolerant resonant dual active bridge converter for more electric aircrafts," in *Proc. IEEE 13th Int. Symp. Power Electron. for Distrib. Gener. Syst.*, 2022, pp. 1–6.
[85] D. Vinnikov, A. Chub, O. Korkh, and M. Malinowski, "Fault-tolerant bidirectional series resonant DC-DC converter with minimum number of components," in *Proc. IEEE Energy Convers. Congr. Expo.*, 2019, pp. 1359–1363.
[86] V. Sidorov, A. Chub, and D. Vinnikov, "Topology morphing control with soft transients for multimode series resonant DC-DC converter," in *Proc. IEEE 22nd Int. Conf. Young Professionals Electron Devices Mater.*, 2021, pp. 331–336.
[87] M. Yilmaz and P. T. Krein, "Review of battery charger topologies, charging power levels, and infrastructure for plug-in electric and hybrid vehicles," *IEEE Trans. Power Electron.*, vol. 28, no. 5, pp. 2151–2169, May 2013.
[88] C. García-Santacruz, P. J. Gómez, J. M. Carrasco, and E. Galván, "Multi P2P energy trading market, integrating energy storage systems and used for optimal scheduling," *IEEE Access*, vol. 10, pp. 64302–64315, 2022.
[89] B. Hussein, A. M. Massoud, and T. Khattab, "Centralized, distributed, and module-integrated electric power system schemes in cubesats: Performance assessment," *IEEE Access*, vol. 10, pp. 55396–55407, 2022.
[90] USB Promoter Group Announces USB Power Delivery Specification Revision 3.1, "Specification defines delivering up to 240W of power over USB type-C," Aug. 15, 2022. [Online]. Available: https://www.usb.org/sites/default/files/2021-09/USB-IF_Cable%20Power%20Rating%20USB4%20Logo%20Announcement_FINAL.pdf
[91] Voltage Classes for Electric Mobility, ZVEI - German Electrical and Electronic Manufacturers' Association Centre of Excellence Electric Mobility, Aug. 15, 2022. [Online]. Available: https://www.zvei.org/fileadmin/user_upload/Presse_und_Medien/Publikationen/2014/april/Voltage_Classes_for_Electric_Mobility/Voltage_Classes_for_Electric_Mobility.pdf
[92] A. Barzkar and M. Ghassemi, "Electric power systems in more and all electric aircraft: A review," *IEEE Access*, vol. 8, pp. 169314–169332, 2020.
[93] B. Sarlioglu and C. T. Morris, "More electric aircraft: Review, challenges, and opportunities for commercial transport aircraft," *IEEE Trans. Transp. Electrific.*, vol. 1, no. 1, pp. 54–64, Jun. 2015.
[94] E. Rodriguez-Diaz, J. C. Vasquez, and J. M. Guerrero, "Intelligent DC homes in future sustainable energy systems: When efficiency and intelligence work together," *IEEE Consum. Electron. Mag.*, vol. 5, no. 1, pp. 74–80, Jan. 2016.
[95] D. L. Gerber, V. Vossos, W. Feng, C. Marnay, B. Nordman, and R. Brown, "A simulation-based efficiency comparison of AC and DC power distribution networks in commercial buildings," *Appl. Energy*, vol. 210, pp. 1167–1187, Jan. 2018.
[96] O. Abdel-Rahim, A. Chub, D. Vinnikov, and A. Blinov, "DC integration of residential photovoltaic systems: A survey," *IEEE Access*, vol. 10, pp. 66974–66991, 2022.
[97] A. Khaligh and Z. Li, "Battery, ultracapacitor, fuel cell, and hybrid energy storage systems for electric, hybrid electric, fuel cell, and plug-in hybrid electric vehicles: State of the art," *IEEE Trans. Veh. Technol.*, vol. 59, no. 6, pp. 2806–2814, Jul. 2010.
[98] Y. Zhao et al., "Characteristic analysis of fuel cell decay based on actual vehicle operating conditions," in *Proc. IEEE 4th Int. Elect. Energy Conf.*, 2021, pp. 1–5.
[99] W. Haoyu and S. Ming, "Variable turns ratio transformer and the LLC isolation controlled resonant converters based on the transformer," China Patent CN 107967986A, Apr. 27, 2018.
[100] W. Haoyu, L. Cheng, and S. Ming, "Restructural H5 inverter bridge and single-direction and dual-direction controlled resonant converter based on the inverter bridge," China Patent CN 109756142A, May 14, 2019.
[101] W. Haoyu and S. Ming, "Voltage-doubling rectifying circuit and application thereof in resonant isolation converter," China Patent CN107171576B, Dec. 12, 2019.
[102] C. Zhang, P. Barbosa, and Y. Jiao, "Three-level modulation for wide output voltage range isolated DC/DC converters," U.S. Patent 011025172B2, Jun. 1, 2021.
[103] C. Zhang and P. Barbosa, "Isolated dc/dc converters for wide output voltage range and control methods thereof," European Patent Office EP3916984A1, Dec. 1, 2021.
[104] J. Itoh and H. Higa, "DC-DC converter," U.S. Patent 10622907B2, Apr. 14, 2020.
[105] L. Ye, H. Dai, and D. Fu, "AC/DC converters with wider voltage regulation range," U.S. Patent 10135350B2, Nov. 20, 2018.
[106] L. Ye, H. Dai, and D. Fu, "AC/DC converters with wider voltage regulation range," U.S. Patent 9973099B2, May 15, 2018.
[107] Y. Zhigang and X. Shengli, "Adaptive wide-output-range variable-gain LLC control circuit," China Patent CN 113098284A, Jul. 9, 2021.

VADIM SIDOROV (STUDENT MEMBER, IEEE) was born in Kazakhstan in 1995. He received the B.Sc. and M.Sc. degrees in power electronics from Novosibirsk State Technical University, Novosibirsk, Russia, in 2017 and 2019, respectively. He is currently working toward the Ph.D. degree in the Power Electronics Group, Tallinn University of Technology, Tallinn, Estonia.

He has coauthored more than 20 papers and one book chapter on power electronics and applications. His research interests include power electronics systems, dc-dc converters, series resonant converters, dc-ac inverters, and electric drive systems.

ANDRII CHUB (Senior Member, IEEE) received the B.Sc. and M.Sc. degrees in electronic systems from the Chernihiv State Technological University, Ukraine, in 2008 and 2009, respectively, and the Ph.D. degree in electrical engineering from Tallinn University of Technology, Tallinn, Estonia, in 2016.

He is currently a Senior Researcher with the Power Electronics Group, Department of Electrical Power Engineering and Mechatronics, Tallinn University of Technology. He was a Visiting Research Fellow with Kiel University in 2017 and a Postdoctoral Researcher with Federico Santa Maria Technical University between 2018 and 2019. He has coauthored more than 100 papers and a book chapter on power electronics and applications and holds several patents and utility models. His research interests include advanced dc-dc converter topologies, renewable energy conversion systems, energy-efficient buildings, reliability and fault-tolerance of power electronic converters.

Dr. Chub is an Associate Editor for the IEEE JOURNAL OF EMERGING AND SELECTED TOPICS IN INDUSTRIAL ELECTRONICS. He was the recipient of numerous best paper awards at IEEE conferences and the 2018 IEEE Industrial Electronics Society Best Conference Paper Award.

DMITRI VINNIKOV (SENIOR MEMBER, IEEE) received the Dipl.Eng., M.Sc., and Dr.Sc.techn. degrees in electrical engineering from Tallinn University of Technology, Tallinn, Estonia, in 1999, 2001, and 2005, respectively.

He is currently the Head of the Power Electronics Group, Department of Electrical Power Engineering and Mechatronics, Tallinn University of Technology. He is the Head of R&D and co-founder of Ubik Solutions LLC—Estonian start-up company dedicated to innovative and smart power electronics for renewable energy systems. Moreover, he is one of the founders and leading researchers of ZEBE—Estonian Centre of Excellence for zero energy and resource efficient smart buildings and districts. He has authored or coauthored 2 books, 5 monographs, and 1 book chapter as well as more than 400 published papers on power converter design and development, and is the holder of numerous patents and utility models in this field. His research interests include applied design of power electronic converters and control systems, renewable energy conversion systems (photovoltaic and wind), impedance-source power converters, and implementation of wide bandgap power semiconductors.

Mr. Vinnikov is a Chair of the IEEE Estonia Section.

FANG Z. PENG (FELLOW, IEEE) received the B.S. degree from Wuhan University, Wuhan, China, in 1983, and the M.S. and Ph.D. degrees from the Nagaoka University of Technology, Nagaoka, Japan, in 1987 and 1990, respectively, all in electrical engineering.

From 1990 to 1992, he was a Research Scientist with Toyo Electric Manufacturing Co., Ltd., Midori, Japan. From 1992 to 1994, he was a Research Assistant Professor with the Tokyo Institute of Technology, Tokyo, Japan. From 1994 to 1997, he was a Research Assistant Professor with the University of Tennessee, Knoxville, TN, USA. From 1994 to 2000, he was a Staff Member with the Oak Ridge National Laboratory, Oak Ridge, TN, USA. From 2000 to 2018, he was a Professor with Michigan State University, East Lansing, MI, USA. In 2018, he joined, as a Professor with the Department of Electrical and Computer Engineering, Florida State University, Tallahassee, FL, USA.